AECOM Imagine it. Delivered.

Alaska-Aleutian tsunami source characterization

January 22, 2019

Prepared for:

Alaska Division of Homeland Security and Emergency Management

Prepared by:

Hong Kie Thio
Principal Seismologist
T: 213.996.2250
E: hong.kie.thio@aecom.com

AECOM
One California Plaza
300 South Grand Avenue
Los Angeles, CA 90071

T: +1 (213) 593 8100
F: +1 (213) 593 8178
aecom.com

Table of Contents

Figures

Tables

1 Introduction

The purpose of this project is to develop source models for tsunami modeling, in particular probabilistic tsunami hazard analysis, for the Alaska-Aleutian Subduction Zone (AASZ). This project was carried out in conjunction with the USGS Powell Center for Tsunami Sources. The final deliverable of this projects is a set of AASZ sources with distributed slip and a rate of occurrence that corresponds to the probabilistic model.

2 Probabilistic framework

The purpose of a hazard analysis is to compute the probability of a certain kind of hazard (e.g., ground shaking, flooding) to reaching or exceeding a certain level. In the simplest case of a probabilistic analysis, the so-called direct method, this can be done by simply tallying observations of the particular hazard at the site. An example of this approach is a hazard curve that is directly obtained from historical observations of water levels. In earthquake related studies, this approach is seldomly used, since it requires a long (relative to the recurrence times) and reliable record of observations, which is rarely achievable. In seismic hazard analyses, it is therefore common to use an earthquake approach, where we compute the ground motions from an earthquake catalog (synthetic or empirical) where every earthquake is defined by a magnitude, location and recurrence rate. For tsunami we follow a similar approach, and the purpose of this study is to provide a framework and earthquake scenario catalog that can be used for probabilistic tsunami hazard analysis. In this work, we only concern ourselves with earthquake sources. From historical observations, we know that submarine landslides also contribute to the tsunami hazard, but these are beyond the scope of this project.

Because of the highly non-linear character of tsunami inundation, and its high computational cost, we have developed a two-step approach to the tsunami hazard analysis at the site. In the first step, we compute a comprehensive probabilistic tsunami hazard analysis for an offshore location near the site, making use of the linear behavior of tsunami in deep water. This allows us to efficiently integrate over thousands of scenarios, which are needed to model the hazard from many different sources.

The methodology behind the seismic equivalent, Probabilistic Seismic Hazard Analysis (PSHA) is well known (e.g., McGuire, 2004), and here we will only briefly describe the adaptations that are made for PTHA. Whereas in PSHA we are usually interested in the exceedance of some ground motion measure such as peak ground acceleration (PGA) or spectral acceleration (SA), in PTHA a parameter of interest (not necessarily the only one) is the maximum tsunami amplitude that is expected to be exceeded at sites along the coast.
The earthquake recurrence models behind the two methods are the same. The difference lies in the process that relates the occurrence of an earthquake with certain magnitude and location to the hazard at the site, such as the Ground Motion Prediction Equations (GMPE) in PSHA. In the empirically derived GMPE, this relationship is a simple function of magnitude and distance, with some corrections applied for source and site characteristics. Because of the aforementioned strong laterally varying nature of tsunami propagation, we have adopted a waveform excitation and propagation approach instead of trying to develop analogous tsunami prediction equations. In fact, current developments in PSHA include the replacement of the GMPEs with ensembles of numerically generated ground motions, which is analogous to the approach proposed here.
The excitation and propagation of tsunamis in deeper water can be modeled using the shallow water wave approximation, which is linear for amplitudes that are significantly smaller than the water depth. We can solve the equation of motion numerically using a finite-difference method, which has been validated to produce accurate tsunami heights for propagation through the oceans, although for very shallow water the amplitudes may become too large, and more sophisticated nonlinear methods are required to model the details of the run-up accurately. Nevertheless, the linear approach provides a very good first approximation of tsunami propagation, taking into account the effects of lateral variations in seafloor depth.

The procedure followed here is similar to the one used for the development of the Tsunami Design Maps that have been introduced in the American Society of Civil Engineer's ASCE 7-16 standard "Minimum Design Loads for Buildings and Other Structures" (ASCE, 2017; Thio et al., 2017).

2.1 Epistemic uncertainty and aleatory variability

An inherent element of a probabilistic analysis is the accounting for limits to our ability of predicting natural processes, either because of a lack of knowledge, referred to as epistemic uncertainty, or because of the random nature of these processes (aleatory variability).

2.1.1 Epistemic uncertainty

Probabilistic tsunami hazard analysis, like its seismic counterpart, follows a dualistic approach to probability. Whereas some aspects are defined in the familiar terms of frequency of occurrence (such as intermediate earthquake recurrence, magnitude distribution), others are more based on judgment, which is a subjective approach (Vick, 2002). For instance, we may characterize the recurrence of intermediate earthquakes in terms of a Gutenberg-Richter distribution, constrained by a catalog of historical earthquakes. The assumption is that the occurrence of earthquakes is a stationary process, and that the catalog represents a homogenous sample of the long-term seismic behavior of a source. For large earthquakes however, the return times are often so long relative to our historic record, even when paleo-seismic data is included, that the recurrence properties of these events cannot be described with a stationary model based on a regression of observed earthquake occurrence. We therefore need to introduce the concept of judgment, where we use our current understanding of earthquake processes, including analyses of similar structures elsewhere, such as local geological conditions, fault geometry, (strain rates etc., to make assumptions on the recurrence and magnitude-area scaling of large earthquakes. This is a subjective or epistemic approach to probability, centered on the observer rather than the observations, and will inevitably be different from one practitioner to another. A rigorous PTHA model therefore includes the use of logic trees to express alternative understandings of the same process, e.g., large earthquake recurrence models, weighted by the subjective likelihood of that alternative model ("degree of belief"), where the weights of the alternatives sum to unity.

2.1.2 Aleatory variability

All aspects of earthquake occurrence and effects contain a measure of natural randomness, even if certain average behavior and measures are clearly identified. This variability is usually expressed in terms of distribution functions around the mean and are included in a PTHA by sampling or integrating over this distribution function. More details on the aleatory variability are discussed in the sections on the various components that contribute to the PTHA.

3 Source characterization

The source characterization for the tsunami models consists of a geometrical characterization of the source, recurrence models for earthquakes that define magnitudes and their recurrence rate, and a generation mechanism for slip distribution on the fault.

3.1 Source geometry

The subduction zone source representations used in this study are based on the Slab2.0 model of Hayes (2018). We fit the depth contours for every subduction zone with a set of quasi-rectangular subfaults that are small enough to represent the slip variability of large tsunamigenic earthquakes. The nominal dimension for these elementary subfaults is 30 km along strike by 10 km in the dip direction but varies according to the curvature of the fault. In order to capture the curvature of the subduction interface, these subfaults are further divided into small patches of 1x1 km. This fine subdivision is strictly meant to accommodate the geometrical complexity; for the actual analysis, the slip on every 30x10 km subfault is uniform.

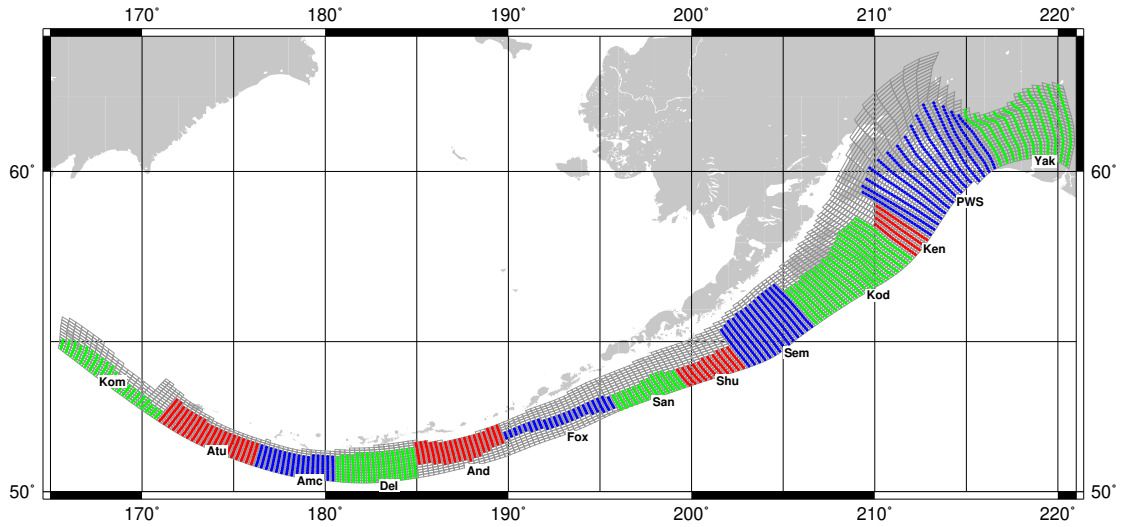

Figure 3-1. Segmentation of the Alaska/Aleutian subduction zone used in this report.

3.2 Earthquake recurrence model

The earthquake recurrence model defines the magnitude of earthquake with their rate of occurrence. In seismic hazard practice the most common magnitude distributions that are used are the (truncated) Gutenberg-Richter (G-R) relation, the Maximum Magnitude (MM) model and the Characteristic Model (CM). Whereas the G-R model is most often used to describe the background seismicity, it is often assumed that the MM and CM models are more appropriate for large faults. In any case, it is important to define the upper limit for the magnitude that can occur on a fault and for this purpose we make use of earthquake scaling relations. For example, for any rupture configuration we can determine the area (A – km^2), which through the published scaling relations (e.g., Skarlatoudis et al. 2016):

$$M = a + b * \log(A)$$

gives us magnitude (M), and thus earthquake moment (M_0 – in Nm):

$$M = \frac{log(M_0) - 9.1}{1.5}$$

The average slip (D) is then obtained through:

$$D = \frac{M}{\mu A}$$

where μ is the elastic shear modulus, we have used a typical crustal value of 30 GPa. In the first equation, the sigma term represents the aleatory variability as the standard deviation of the distribution around the mean. The three

parameters are given in **Table** 3**-**1. We approximate this distribution using a discrete set of alternative values (-2σ, -σ, median, +σ, +2σ) with weights derived from the normal distribution (.4, .24 and .06 for median, ±σ and ±2σ respectively.

Various authors have developed scaling relationship for subduction zone earthquakes, which vary significantly due to different assumptions and regression models used. In order to take these different views of the earthquake scaling relations into account, we have applied several logic tree branches that represent these different models. In **Figure** 3**-**2 we have plotted several recent scaling relations as well some data from Alaskan earthquakes. None of the relations fir the Alaska data particularly well, but it does appear that a self-similar relation (b=1.0) would be more appropriate. We bracket the data with the data with the Ye, Murotani and Skarlatoudis relations. The equally weighted models we considered are from Skarlatoudis et al. (2016), Ye et al. (2019) and Murotani (2008, 2013) (**Table** 3**-**1). While the equal weighting tends to skew the results towards a somewhat lover magnitude compared to the Alaska data, we find that this is a more common characteristic of most models and our weighting is thus a compromise to the much larger global datasets and the more soure-specific but smaller dataset.

Scaling relation	a	b	σ	Weight
Skarlatoudis	3.685	1.0	0.176	1/3
Murotani	3.980	1.0	0.037	1/3
Ye	4.1333	1.0	0.2	1/3

Table 3-1 Scaling relations used to relate magnitude with rupture area.

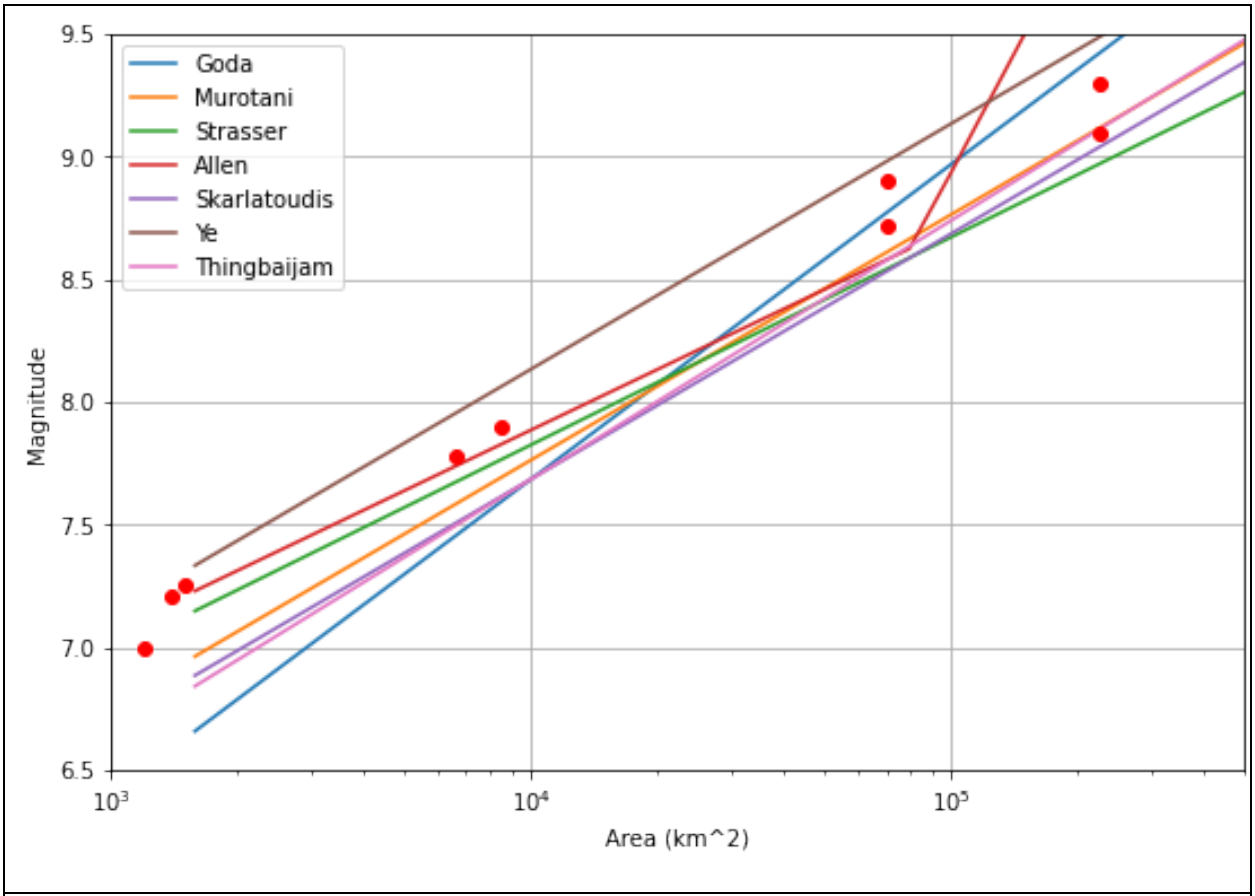

Figure 3-2. Area-magnitude scaling relations for subduction zone interface earthquakes.

3.3 Generation of slip models

While in earlier analyses (e.g., Thio et al., 2010), we have used uniform slip models to produce tsunami waves. At local distances however, the slip variability is an important factor and asperities with large amounts of slip can cause significantly higher tsunami waves, especially locally, as is illustrated by the recent Tohoku earthquake where the maximum slip exceeded the average slip by at least a factor of 2. Murotani et al. (2008) studied the slip distributions of several subduction zone earthquakes and found a ratio of maximum slip over average slip of 2.2. To include this aleatory slip variability, we used variable slip rupture models with one third of the rupture as an asperity with twice the average slip and the other two-thirds of the rupture at half the average slip. In order to achieve uniform long-term slip, we computed a total of three scenarios for each event where the asperity occupies every part of the rupture once. This way, we avoid the risk that in some areas the hazard is over- or under-estimated due to incomplete or overlapping asperity coverage offshore.

3.4 Segmentation

3.4.1 The ASCE 7-16 model

When the ASCE 7-16 tsunami hazard maps were developed the most recent Alaska source model from the USGS was already a decade old, and a significant amount of new data had been published since. The logic tree consists of a segmented model only (based on Jacobs and Nishenko, 1990), with multiple segment ruptures allowed (**Figure** 3-3). The model is weighted towards the single-segment ruptures (0.6) with 2-3 segment ruptures at 0.3 and very large multi-segments with a weight of .1. Scaling relations used were Murotani (2008), Strasser et al. (2010) and Papazachos et al. (2004) with equal weights. The segmentation corresponds with observed rupture boundaries from historical earthquakes (Jacobs and Nishenko, 1990; Figure 3-4) but other authors have concluded that larger multi-segment ruptures are viable scenarios as well (Table 3-2).

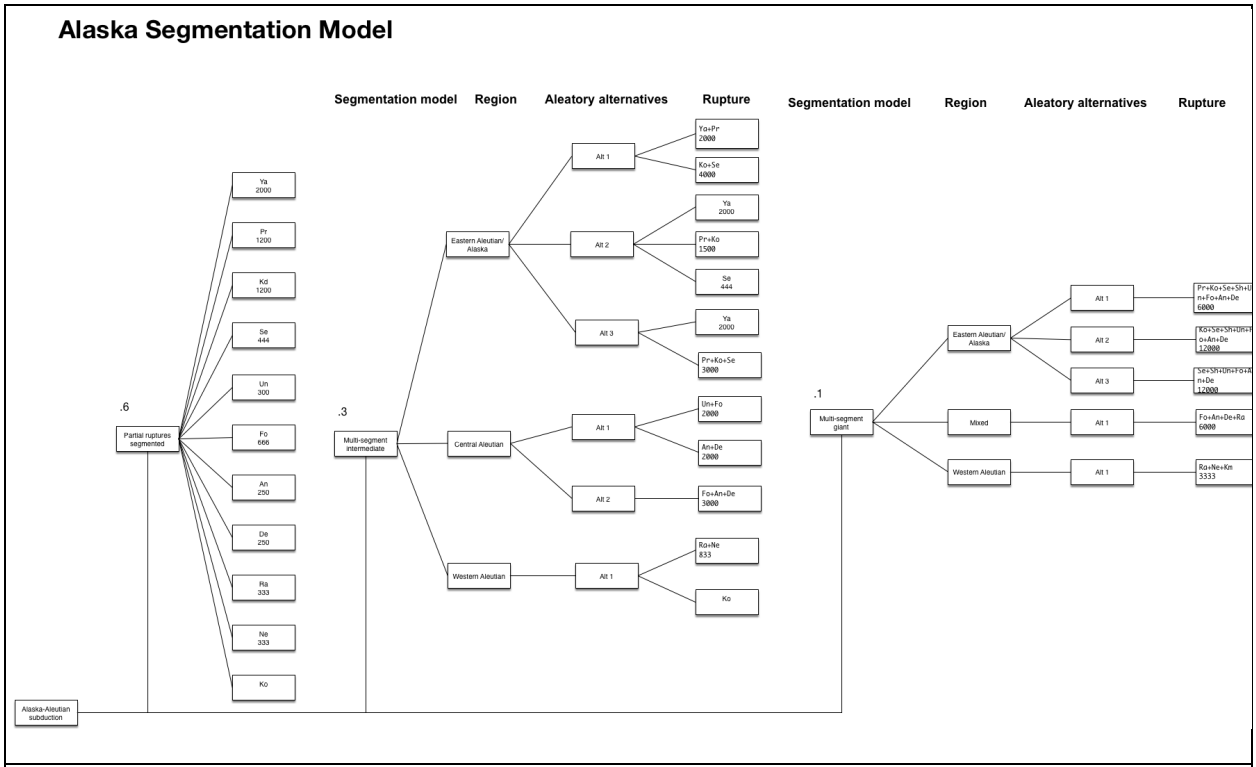

Figure 3-3. Partial logic tree showing the different branches for the segmentation of the Alaska/Aleutian subduction zone used in ASCE 7-16.

The numbers at each branch are relative weights given to that branch.

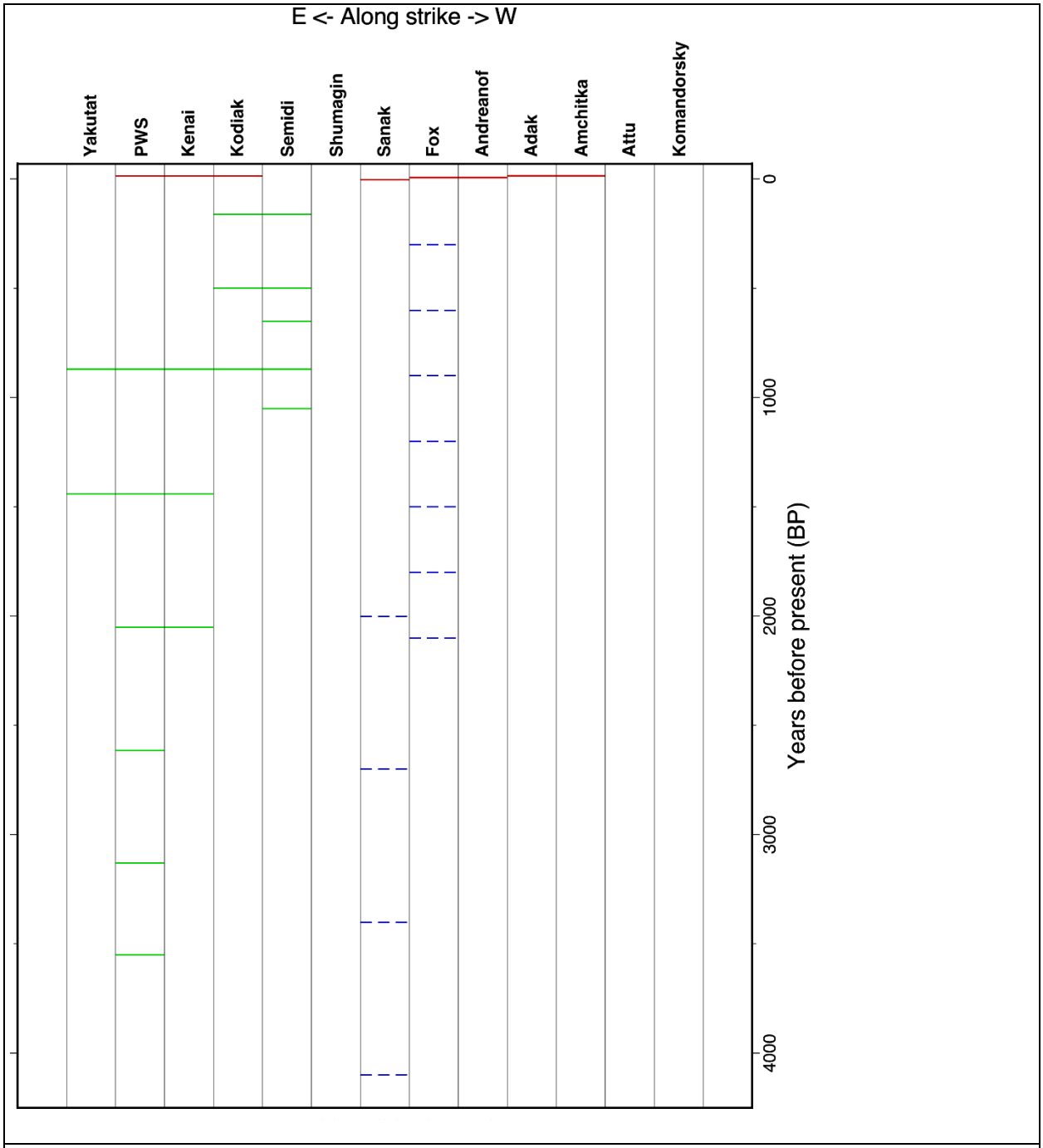

Figure 3-4 Record of large events along the Alaska-Aleutian subduction zone

Segmentation model			**Year of Historical Events**								
Nishenko & Jacobs (1990)	Wesson et al. (2007)	McCaffrey (1997)	1849	1899	1917	1938	1946	1957	1964	1965	**1986**
Yakataga	Yakataga	Alaska		+							
Prince-William Sound	Prince-William Sound								+		
Kodiak	Kodiak								+		
Semidi	Semidi					+					
Shumagin	Shumagin				-						
Unimak	Western Aleutian	Eastern Aleutians					+				
Fox Island							-				
Andreanof											+
Delarof								+			
Rat Island		Western Aleutians								+	
Near Island										+	
Komandorsky	Komandorsky		+								

Table 3-2 Segmentation models of the Alaska-Aleutian subduction zone and the extent of recent large earthquakes. + means the entire segment ruptures, - means partial rupture

3.4.2 Updated segmentation logic tree

In 2019, a USGS Powell Center workshop on tsunami sources for Alaska was organized with the aim of developing an updated community source model for the Alaska/Aleutian subduction zone. Although this effort is still ongoing, we have included the early results from this workshop into our model as well, as a separate branch of the logic tree. This alternative has an updated multi-segment rupture model and also includes a branch where earthquake can occur along the entire subduction ("floating sources") irrespective of any segmentation but primarily constrained by local slip rates. In practical terms, this last alternative extends the magnitude range to smaller vents compared to the original ASCE7-16 model. A partial logic tree of the different branches is shown in Figure 3-5.

The first branch point (Figure 3-5) concerned the question whether ruptures are thought to follow the current segmentation model (including multi-segment ruptures) or whether ruptures follow a floating model where they can occur anywhere irrespective of segment boundaries. These two branches were thought to be roughly equal in probability. In this paper we follow the segmented rupture branch with the floating rupture branch to be defines at a later stage. The basic premise of a segmentation model is that there are certain physical/geometrical properties of the subduction zone interface (including the overriding and subduction plates) that act as natural inhibitors to earthquake rupture propagation. Whether or not these boundaries are in fact pervasive in time remains to be seen, as we have limited direct observations of ruptures in the AASZ given the short time span of historical observations. The current boundaries are primarily based on the rupture extent of recent large earthquakes on the AASZ (e.g., Jacobs and Nishenko, 1990) as well as more recent geodetic observations and modeling (e.g., Cross and Freymuller, 2008). Our current model differs in a few ways from the ASCE 7-16 model with an extra segment (Kenai) between the Kodiak and Prince William Sound segments as well as some changes in the location of the segment boundaries.

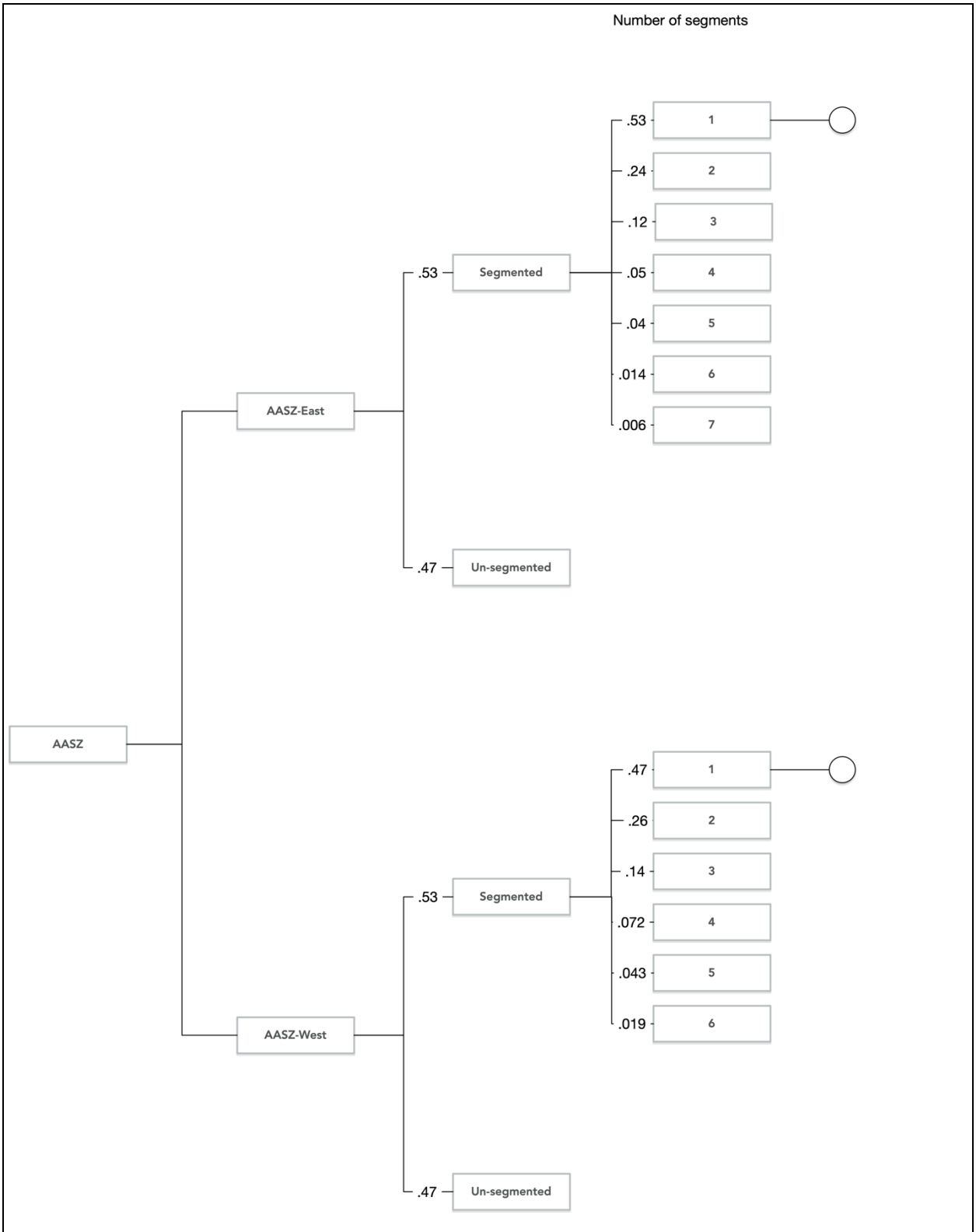

Figure 3-5 Basic branches of the AASZ logic tree produced by the Powell center workshop. The branches on the right are further expanded in the following figures.

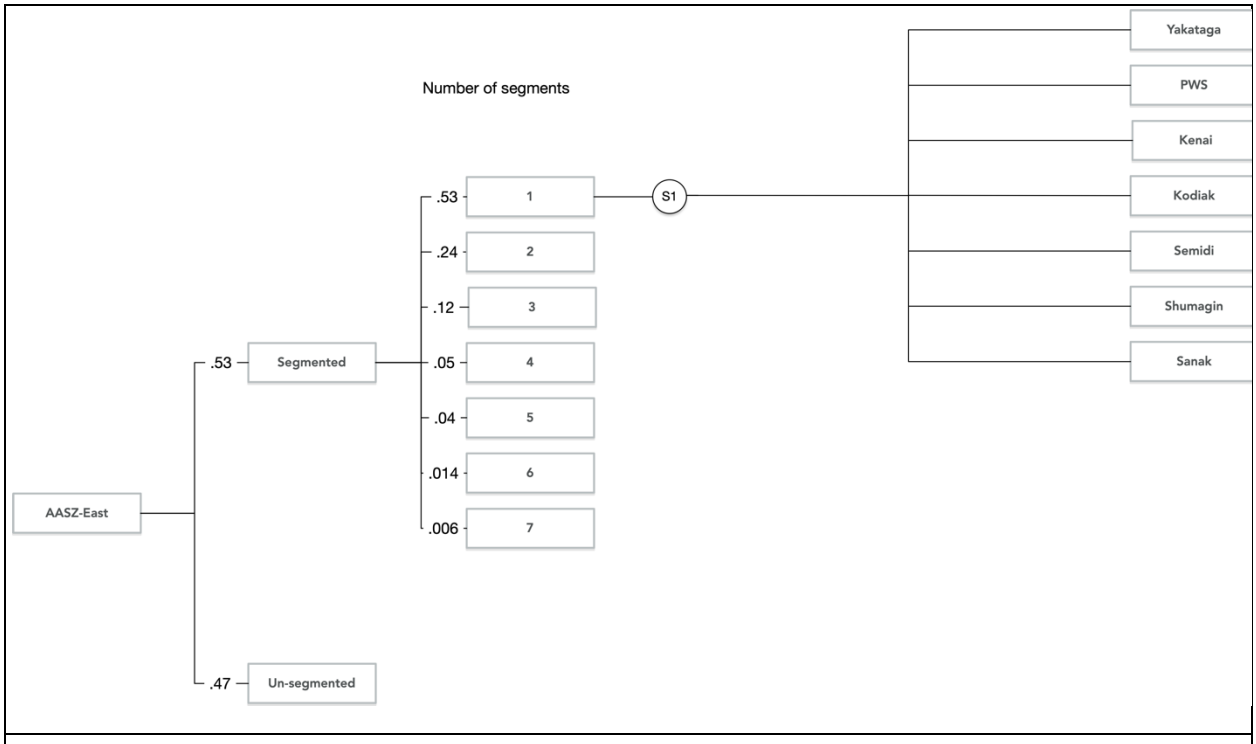

Figure 3-6 Single Segment branch of the AASZ logic tree produced by the Powell center workshop.

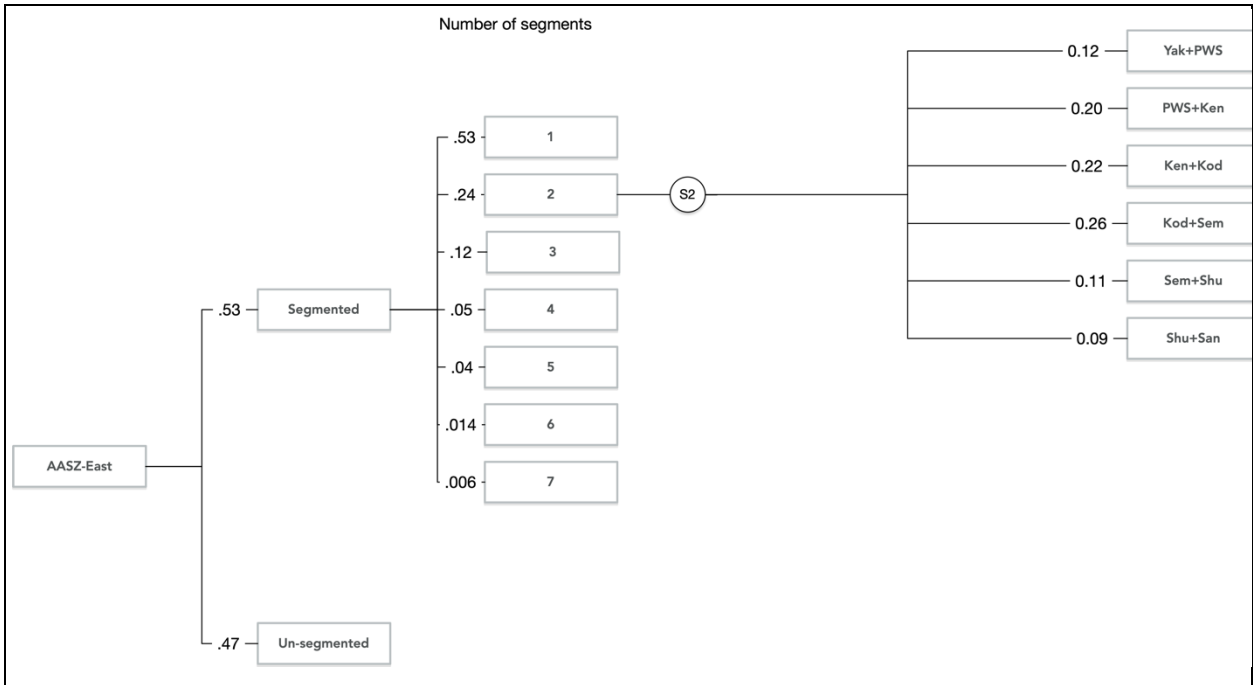

Figure 3-7 Two Segment branch of the eastern AASZ logic tree produced by the Powell center workshop.

3.5 Event rates

Earthquake rates can be defined in several ways: directly from empirical observations (e.g., earthquake catalogs), or derived from physical models of the Earth. When using earthquake catalogs, it is common to fit the earthquake magnitude occurrences in time using an exponential function (decaying with increasing magnitude), such as the Gutenberg-Richter relations. For larger earthquakes it is common to assign earthquake recurrence times directly to the earthquake scenarios based on observed earthquake interval times. The historical record of earthquakes in Alaska is very short, although when paleo-seismic data is included, it can stretch into thousands of years back. Unfortunately, the observations are still very sparse, and for pre-historic earthquakes, it is currently not possible to unambiguously distinguish between a sequence of earthquakes along the AASZ, or a single very large one. Independent estimates of the size of these events are often not available. Because of these problems, we are using simple models of earthquake recurrences based on plate convergence models, geodetic observations, and event recurrence times where available.

3.5.1 Plate model

The overall plate configuration of the AASZ is relative straightforward with the Pacific Plate subducting under the North American Plate. But with the large extent and geometry of the AASZ, there are significant changes in the convergence along strike, with trench normal rates ranging from almost zero in the west to 70 mm/yr in the central and eastern AASZ. Additionally, in the west where the convergence is oblique, there is evidence for strain partitioning with one or more micro-plates along the chain bounded by the AASZ to the south and strike-slip faults to the north.

The plate rates along the AASZ are summarized in Table 3-3.

3.5.2 Geodetic observations and seismic coupling

Plate rates are only one element in the determination of the recurrence properties of the earthquake set. Often, a significant part of the slip rate on subduction zone interfaces is accommodated by aseismic slip, or creep. Such behavior reduces the effective slip rate by a factor called the seismic efficiency or coupling coefficient (the fraction of the slip that is accommodated in seismic events).

By comparing plate model rates with local observed geodetic strain rates, and assuming interface geometry that separates the overriding and subducting plate, it is possible to deduce the coupling coefficient on the interface as was done by Cross and Freymuller (). Our current model is based on this approach and

Table 3-3 Summary of tectonic parameters for the AASZ from geologic and geodetic data per segment.

Segment	Length (km)	Width (km)	Av. geologic recurrence interval (yr)	Convergence rate (mm/yr)		Slip deficit (%)	User efficiency	Coupling width (km)	Coupling area	Mmax	Av. slip/event	Return period	Data	Ref.
				Pac-Arc	Pac-Arc GPS									
Yakataga	250	215	750	57	57	50	50	350	49392.76	8.57	5.80	203.61	G, P, S, T	E20, Sh09a, Sh09b
PWS	240	400	590	59	59	100	100	200–300	126018.95	9.10	13.79	233.80	H, G, P	E20, Sh14a, SF09
Kenai	110	335	516	61	61	100	100	100	16956.34	7.98	2.16	35.40	G, P	E20, K05, Sh18, SF09
Kodiak	425	270	295	63	63	100	100	175	77823.94	8.83	8.83	140.23	H, G, P	B14, E20, Sh14a, SF09
Semidi	255	135	212	66	66	100	100	200	53714.32	8.62	6.27	95.01	H, G, P	E20, N15
Shumagin	225	110	>3400	68	68	20–40	30	100	24754.99	8.19	3.06	150.20	H, G, P	E20, W14
Sanak	285	80	2000	69	70	2	2	65	21778.63	8.12	2.72	1972.33	H, G, P	E20
Fox	435	75	210	71	72	46–100	73	75	42387.71	8.49	5.04	97.20	H, G, P	E20, W16, W19
Andreanof	370	75	nd	70	75	100	100	30	27077.43	8.24	3.33	47.56	H, G	C08, F08
Adak	325	75	nd	66	70	25	25	75	36950.16	8.41	4.44	268.92	H, G, S	C08, F08
Amchitka	330	70	nd	59	68	nd?	50	nd?	28423.57	8.27	3.48	118.02	H, G, S, T	C08, F08, G88
Attu	405	65	nd	51	65	62	62	85	36307.11	8.40	4.37	138.07	H, G, S, T	C08, F08, G88
Komandorsky	560	80	nd	47	38	100	100	40	36395.16	8.40	4.38	93.10	S, T	C08, G88

Average of maximum and minimum widths measured from trench to 40 km contour depicted in Slab 2 (Hayes et al., 2018). Width of the Yakataga fault section measured from trench to 20 km contour.
Data that defines fault section: G, geodesy; H, historical seismicity; P, paleoseismology; S, forearc structure; T, topography. This table has been compiled by R. Briggs and J. Freymueller and the current author.
References: eB14, Briggs et al. (2014); C08, Cross and Freymueller (2008); E20, Elliott and Freymueller (2020); F08, Freymueller et al. (2008); G88, Geist et al. (1988); K15, Kelsey et al. (2015); N15, Nelson et al. (2015); N16, Nicolsky et al. (2016); Sh09a, Sh09b, Sh14a, Sh14b, Sh16, Sh18, Shennan et al. (2009a, 2009b, 2014a, 2014b, 2016, 2018); SF09, Suito and Freymueller (2009); W14, W16, W19, Witter et al. (2014, 2016, 2019).

3.6 Slip distributions

Slip tends to be heterogeneously distributed for every earthquake, and the slip distribution displays both random variations as well as systematic patterns. Systemic patterns are due to underlying physical conditions such as rheology and elastic behaviour whereas random (aleatory) patterns are more unpredictable due to the randomness of earthquake processes. The aleatory variability in slip average out to the long-term (systematic) slip distributions. An example of the systematic variation is the variation of slip with depth due to depth-dependent elastic behaviour. Along strike there are several factors that can lead to systematic differences in fault slip (Table 3-3):

- Variations in slip rate – along the length of the AASZ, the effective slip rate varies considerable due to changes in plate rates and interface geometry as well as seismic coupling
- Variations in coupling – geodetic data indicates that the coupling varies along strike, leading to a change in effective slip rates
- Variation in fault width – if the maximum slip follows a static stress drop model, then the differences in fault width will also results in differences in maximum slip along the subduction zone.

It should be noted that these along-strike variations can be accommodated by systematic slip patterns per scenario, but also by different earthquake statistics along strike. In our model these two effects are included implicitly by the way the slip distributions are computed and by the final weighting of the different scenarios.

Short-term (stochastic) slip variability refers to the differences in slip distribution between individual earthquakes. Individual earthquake slip distributions tend to be quite heterogenous with areas of high slip (asperities) and areas with relatively low slip. Murotani (2008) studied the statistics of maximum vs. average slip and found that on average the maximum slip amounts to twice the average slip. In order to account for the variability, we represent any magnitude earthquake with three different instances where one-third of the rupture is an asperity with twice the average slip and the remaining area with half the average slip. The location of the asperity is either at one of the ends of the rupture or in the center, so that the entire plane is subjected to the maximum slip. The rate of occurrence of these events is simply one-third of the rate of the original event.

Earthquake slip also varies with depth. In the long-term, slip tends to taper with depth as the increasing temperatures and pressures result in a more ductile regime. In our slip models, we apply a cosine taper with depth. Since the deep slip is less consequential for tsunami generation, we do not use a separate asperity distribution with depth. The depth distribution closely follows the long-term slip characteristics.

3.6.1 Logic tree branches for slip with depth

The width of the rupture planes is another source of epistemic uncertainty. On the trenchward side, we consider both ruptures that break all the way to the trench as well as ruptures that terminate in the accretionary prism. For the AASZ, we don't have sufficient data to constrain these models, so we assigned equal weights to the trench-breaking and buried alternatives.

3.7 Weighting of individual sources

The source characterization that we propose here is as follows;

For every subfault i we determine an effective slip rate R_i. this slip rate is mostly based on the geodetic coupling models of Cross et al. (2014, 2020, etc.).
For all rupture extents we develop slip distributions based on a set of rules. These rules contain characteristics of observed rupture. They may be as simple (as in the current case) as dimensions of asperities and tapering of slip towards the edges of the rupture area, but in a more sophisticated manner can be statistical parameters that have been obtained from a regression of megathrust earthquake slip models (e.g., Murotani, Skarlatoudis et al.), applied to stochastic models (Pitarka and Graves., Leveque et al.).

These various methods can lead to a large number of slip models (scenarios), even for a single segment. In order to calculate rates for every scenario, an inversion procedure (e.g., Andrews and Scherer, 2000) is used to make sure that the cumulative slip rates are consistent with the desired slip rates per subfault.

3.7.1 Inversion procedure

For the inversion we use a non-negative least squares routine (Lawson and Hansen, 1974) in the following way:

$$\begin{pmatrix} S_{1,1} & \cdots & \cdots & S_{1,ne} \\ S_{2,1} & & & \\ \vdots & & & \\ 0 & & & \\ 0 & & & \\ \vdots & & & \\ S_{ns,1} & & & S_{ns,ne} \end{pmatrix} \begin{pmatrix} W_1 \\ \\ \\ W_{ne} \end{pmatrix} = \begin{pmatrix} R_1 \\ \\ \\ R_{ns} \end{pmatrix}$$

Here, the $S_{i,j}$ represents the slip at subfault i (out of ns total subfaults) for scenario j. Since ns is the total number of subfaults that are capable of rupturing in this particular logic tree branch, and typically all subfaults of the AASZ, a lot of $S_{i,j}$ will be zero. R_i is the target slip rate for subfault i. The weights W_j define the actual slip rate for every scenario j, and are solved for using the inversion procedure.

Additional constraints such as paleoseismic recurrence rates and the workshop weights are added to the scheme as additional below the regular normal equations. In our current scheme, because of the limited degrees of freedom, the inversion results are close to the original input weights since they were already constrained per segment to conform to the overall slip rates. The addition of the multi-scenario events only changed the complexity slightly because of their low weights. However, as more complexities are added to the schema, such as stochastic sources or floating ruptures, the inversion will make a significant impact in the weighting of the individual scenarios.

4 Rupture scenarios

The logic tree presented in this report resulted in 4932 unique rupture scenarios and associated event rates. Figure 4-1 shows some examples of slip distribution patterns for single and multi-segment scenarios along the AASZ. These models are available on the GitHub site (see appendix A). These scenarios are characterized by a set of rectangular fault elements with their centroid location (lat/lon/depth), orientation (strike/dip/slip) length (horizontal) and width (downdip) and amount of slip (meters). For every scenario, we have computed a return time based on the logic tree and Table 3-3. These return period should be used in in the context of the full set of events and are meaningless on their own. To find scenarios that are representative for particular return periods, the inverse return periods (rates) for all the events that are represented by the single event need to be added.

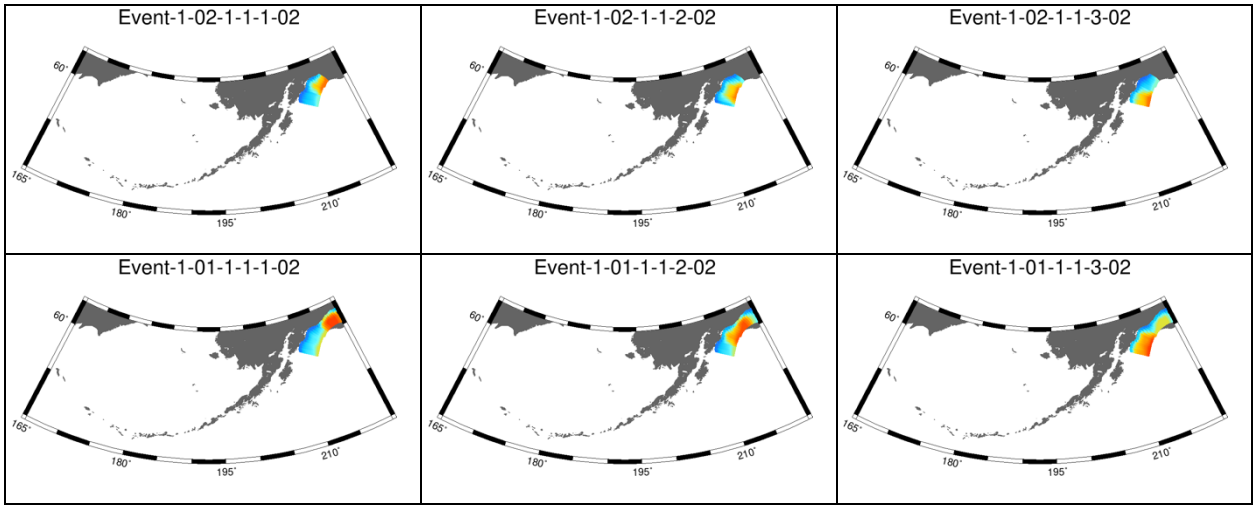

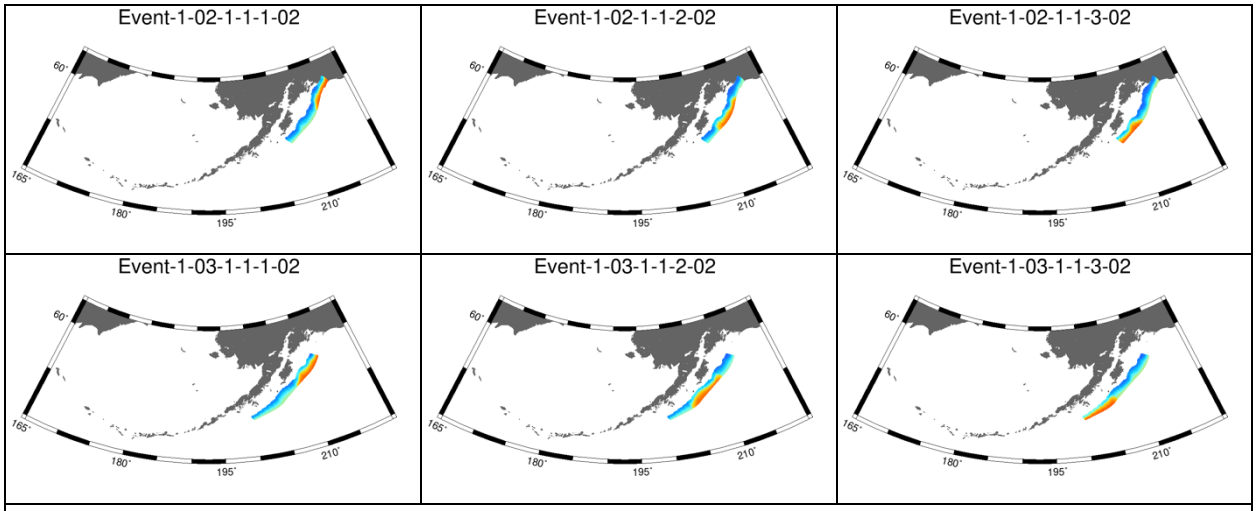

Figure 4-1 Examples of slip distributions for single-,double-, triple- and quadruple-segment ruptures (top to bottom row respectively) with the three different asperity locations (left to right columns).

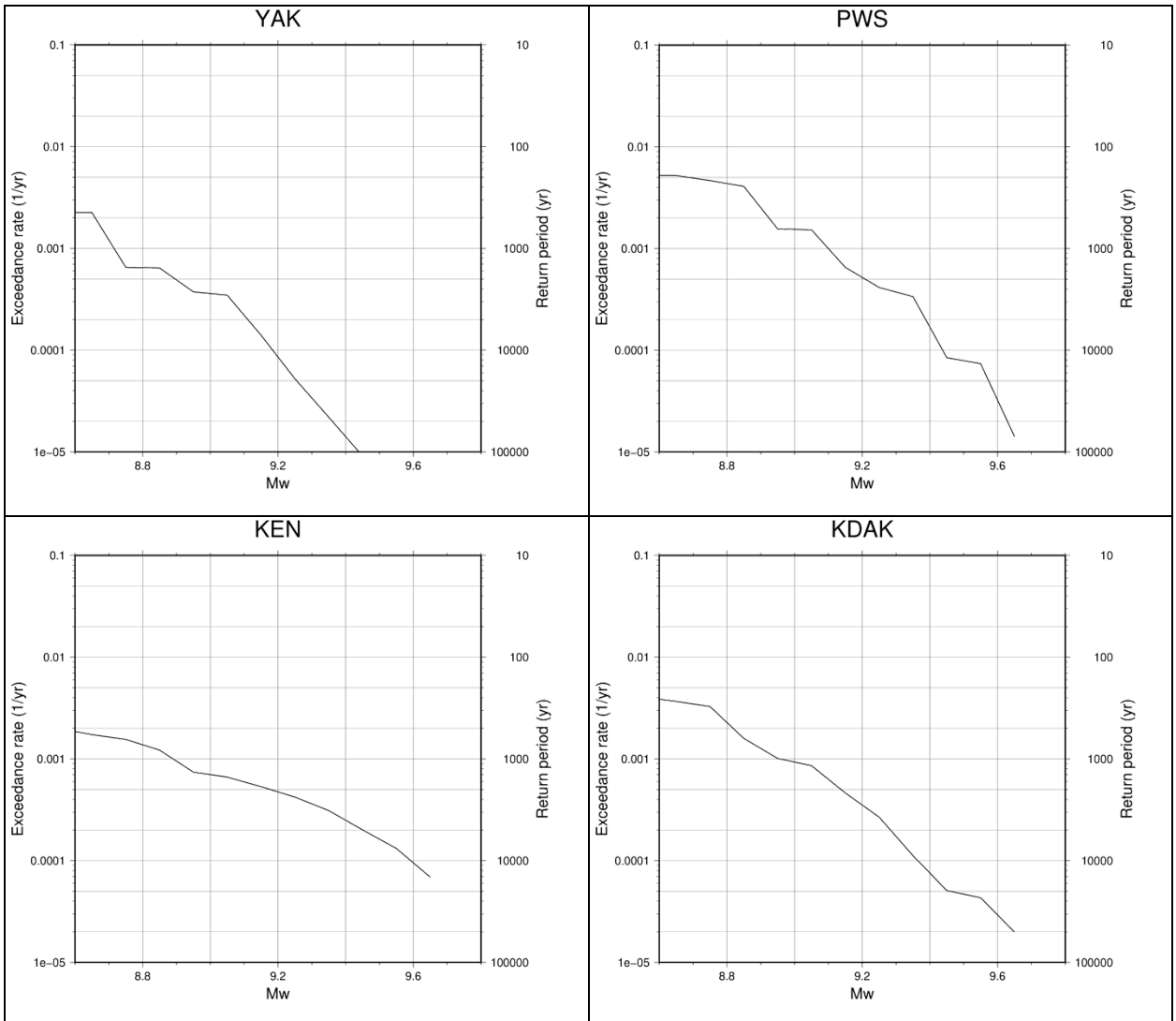

Figure 4-2 Cumulative magnitude recurrence relations for the four eastern segments.

The cumulative return period distributions of earthquake magnitude for every segment are shown in Figure 4-2 through Figure 4-4. These distributions represent any earthquake in our model where the particular segment participates. These return periods are consistent with the overall coupling rates from Table 3-3. Table 3-3 Summary of tectonic parameters for the AASZ from geologic and geodetic data per segment.

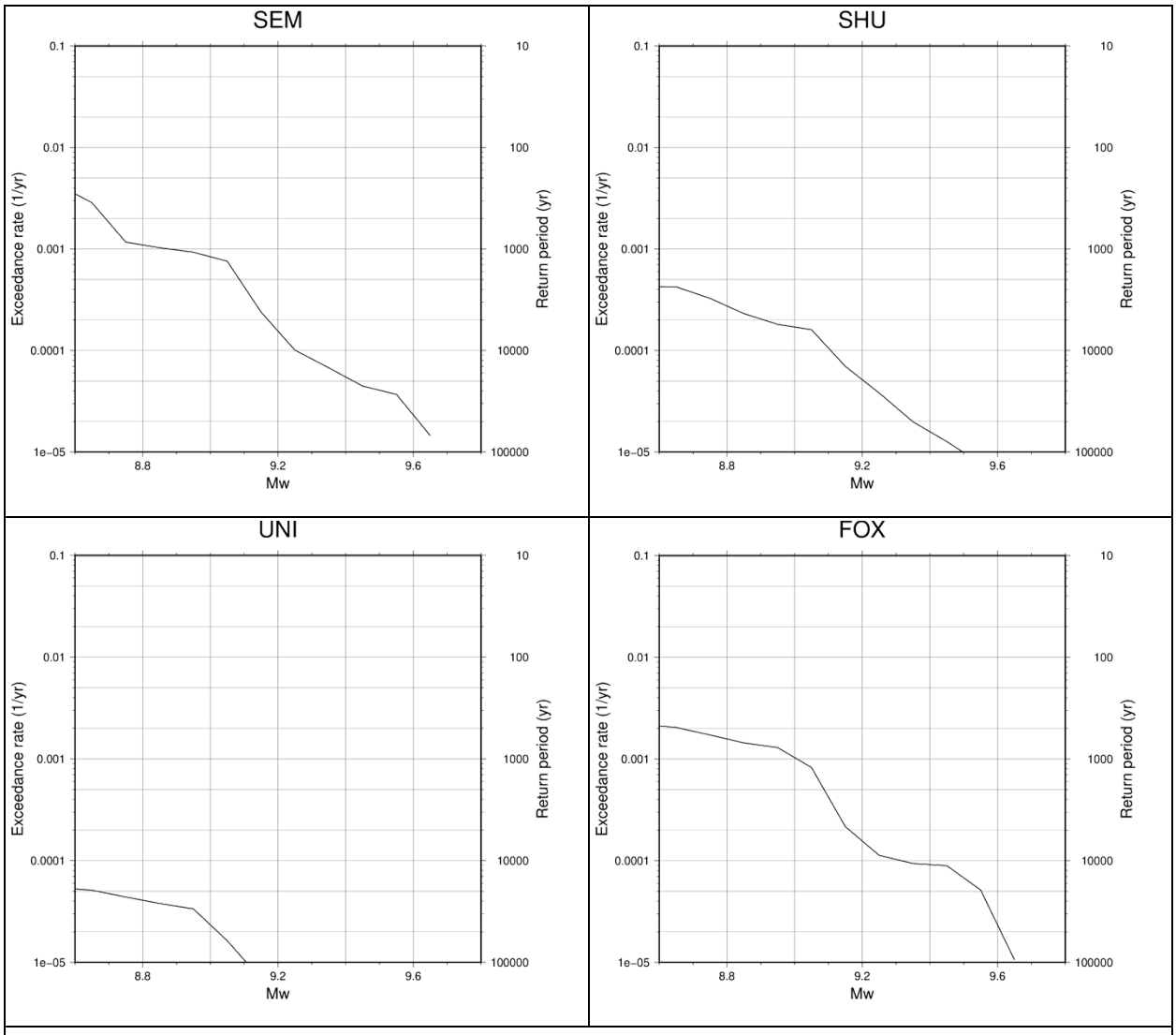

Figure 4-3 Cumulative magnitude recurrence relations for the four central segments.

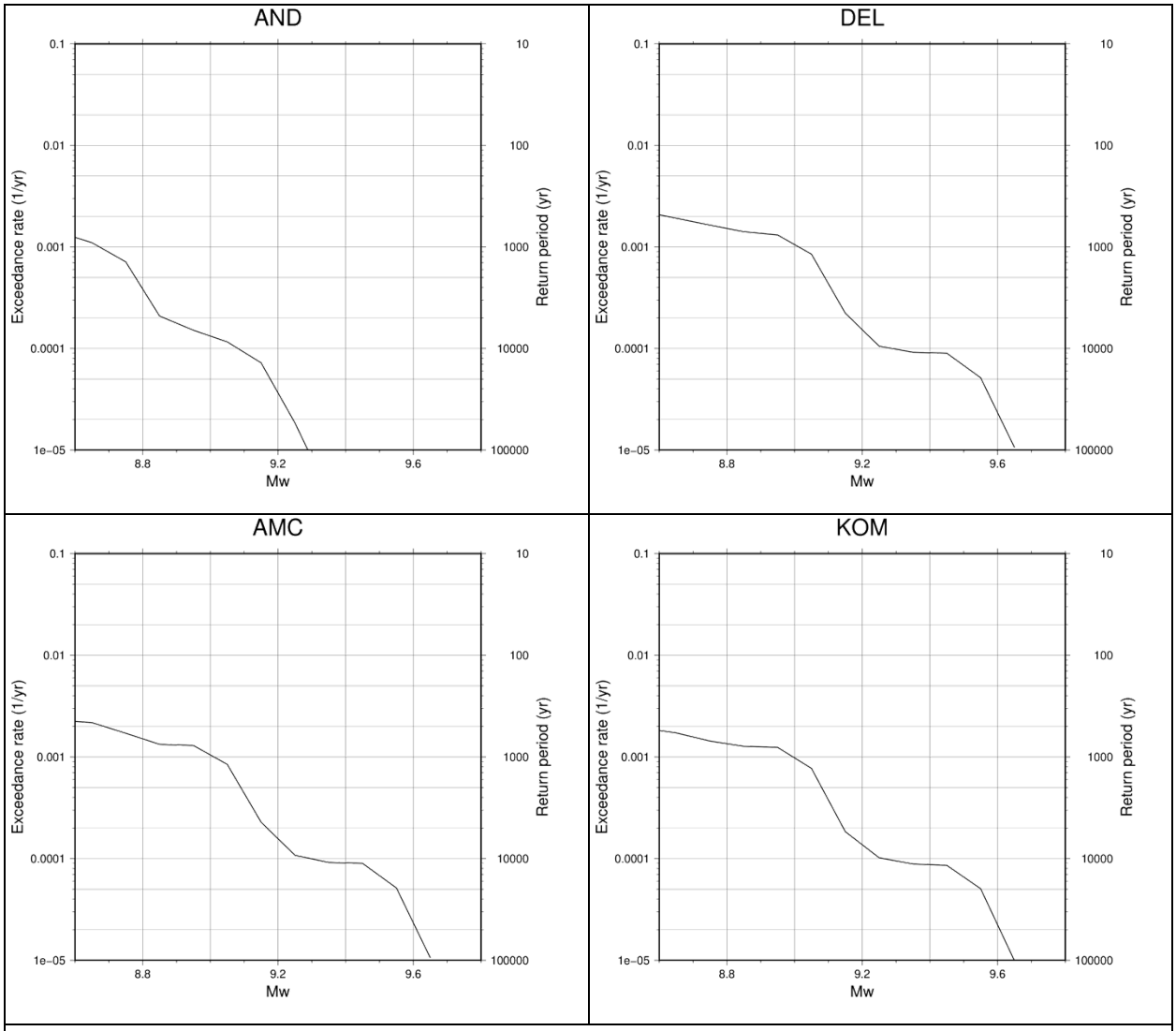

Figure 4-4 Cumulative magnitude recurrence relations for the four western segments.

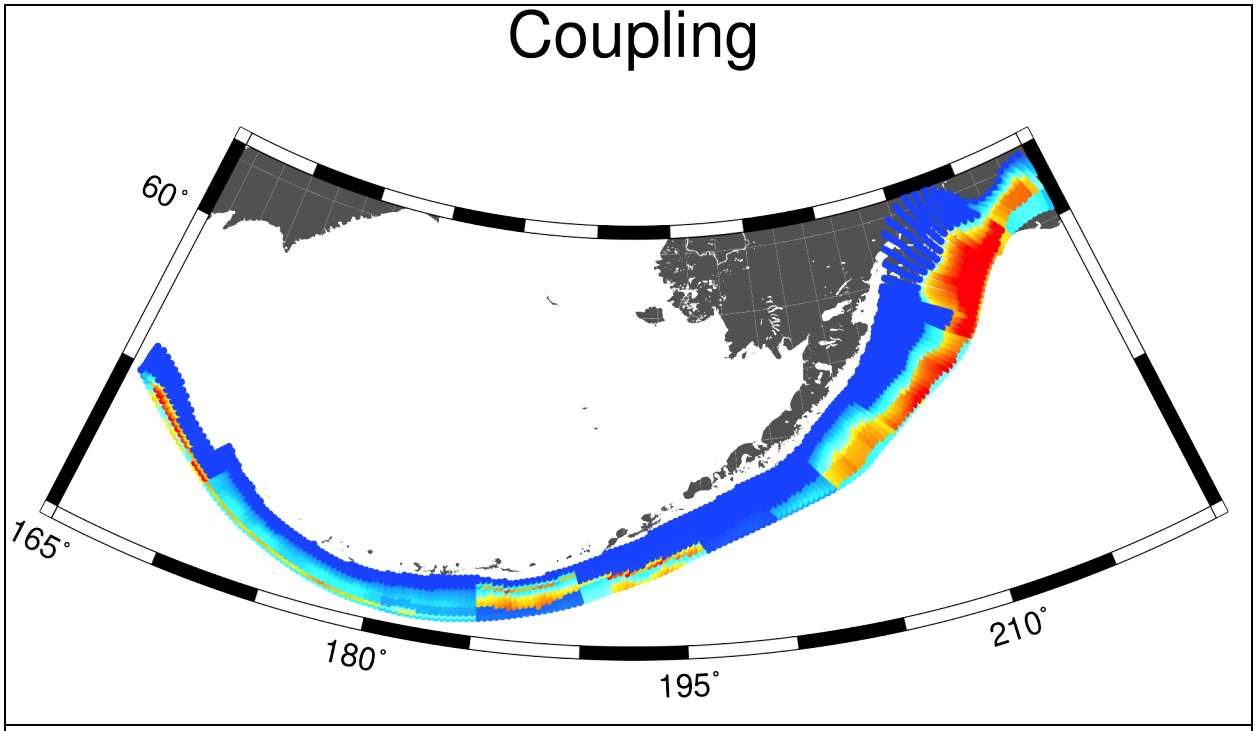

Figure 4-5 Coupling coefficients for the final logic tree model.

5 Data and software dissemination

The rupture scenarios, event rates and associated software currently available through Github:

https://github.com/hkthio/PHA. Explanations of the file formats are included on that site and in Appendix A. The software used to derive these sources is included, and we are in the process of adding the software needed for the full probabilistic analysis.

6 References

American Society of Civil Engineers (ASCE), 2017. *Minimum Design Loads and Associated Criteria for Buildings and Other Structures (ASCE/SEI 7-16).*

Annaka, T., Satake, K., Sakakiyama, T., Yanagisawa, K., and Shuto, N., 2007. Logic-tree Approach for Probabilistic Tsunami Hazard Analysis and its Applications to the Japanese Coasts. *Pure and Applied Geophysics* **164**(2-3), 577–592.

Blaser, L., Kruger, F., Ohrnberger, M., and Scherbaum, F., 2010. Scaling Relations of Earthquake Source Parameter Estimates with Special Focus on Subduction Environment. Bulletin of the Seismological Society of America, 100, no. 6, p. 2914–2926, doi: 10.1785/0120100111.

Brown, J.R., Prejean, S.G., Beroza, G.C., Gomberg, J.S., and Haeussler, 2013. Deep low-frequency earthquakes in tectonic tremor along the Alaska-Aleutian subduction zone, *J. Geophys. Res. Solid Earth*, *118*(3), 1079–1090, doi:10.1029/2012JB009459.

Cross, R.S. & Freymueller, J.T. (2007) Plate coupling variation and block translation in the Andreanof segment of the Aleutian arc determined by subduction zone modeling using GPS data. *Geophys. Res. Lett.*, **34**, 1653–5. doi:10.1029/2006gl028970

Cross, R.S. & Freymueller, J.T. (2008) Evidence for and implications of a Bering plate based on geodetic measurements from the Aleutians and western Alaska. *J. Geophys. Res. Solid Earth*, **113**, 830–19. doi:10.1029/2007jb005136

Cross, R.S. & Freymueller, J.T. (2008) Correction to “Evidence for and implications of a Bering Plate based on geodetic measurements from the Aleutians and western Alaska.” *J. Geophys. Res. Solid Earth*, **113**, B10404-1. doi:10.1029/2008jb006104

Elliott, J. & Freymueller, J.T. (2020) A Block Model of Present-Day Kinematics of Alaska and Western Canada. *J. Geophys. Res. Solid Earth*, 1–77. doi:10.1029/2019jb018378

Fournier, T.J. & Freymueller, J.T. (2007) Transition from locked to creeping subduction in the Shumagin region, Alaska. *Geophys. Res. Lett.*, **34**, L06303. doi:10.1029/2006gl029073

Hayes, G., 2018, Slab2 - A Comprehensive Subduction Zone Geometry Model: U.S. Geological Survey data release, https://doi.org/10.5066/F7PV6JNV.

Johnson, J.M., Satake, K., Holdahl, S.R., and Sauber, J., 1996. The 1964 Prince William Sound earthquake: Joint inversion of tsunami and geodetic data. *Journal of Geophysical Research: Solid Earth* **101**, 523–532.

McGuire, R.K., 2004. Seismic hazard and risk analysis, Earthquake Engineering Research Institute, MNO-10, 240 pp.

Murotani, S., Miyake, H., and Koketsu, K., 2008. Scaling of characterized slip models for plate-boundary earthquakes. *Earth, Planets and Space* **60**(9), 987.

Murotani, S., Satake, K., and Fujii, Y., 2013. Scaling relations of seismic moment, rupture area, average slip, and asperity size for M~9 subduction-zone earthquakes. *Geophysical Research Letters* **40**(19), 5070–5074.

Nelson, A.R., Briggs, R.W., Dura, T., Engelhart, S.E., Gelfenbaum, G., Bradley, L.-A., Forman, S.L., Vane, C.H., and Kelley, K.A., 2015. Tsunami recurrence in the eastern Alaska-Aleutian arc: A Holocene stratigraphic record from Chirikof Island, Alaska. *Geosphere* **11**(4), 1172–1203.

Nishenko, S.P., and Jacob, K.H., 1990. Seismic potential of the Queen Charlotte-Alaska-Aleutian Seismic Zone. *Journal of Geophysical Research: Oceans* **95**(B3), 2511–2532.

Papazachos, B., Scordilis, E., Panagiotopoulos, D., Papazachos, C.B., and Karakaisis, G.F., 2004. Global relations between seismic fault parameters and moment magnitude of earthquakes, *Bulletin of the Geological Society of Greece*, *36*(3), 1482–1489.

Petersen, M.D., Moschetti, M.P., Powers, P.M., Mueller, C.S., Haller, K.M., Frankel, A.D., Zeng, Yuehua, Rezaeian, Sanaz, Harmsen, S.C., Boyd, O.S., Field, Ned, Chen, Rui, Rukstales, K.S., Luco, Nico, Wheeler, R.L., Williams, R.A., and Olsen, A.H., 2014, Documentation for the 2014 update of the United States national seismic hazard maps: U.S. Geological Survey Open-File Report 2014–1091, 243 p., *https://dx.doi.org/10.3133/ofr20141091*.

Plafker, G., 1965. Tectonic Deformation Associated with the 1964 Alaska Earthquake. *Science* **148**(3678), 1675–1687.

Shennan, I., Bruhn, R., and Plafker, G., 2009. Multi-segment earthquakes and tsunami potential of the Aleutian megathrust. *Quaternary Science Reviews* **28**(1-2), 7–13.

Schwartz, S.Y., 1999. Non-characteristic behavior and complex recurrence of large subduction zone earthquakes. *Journal of Geophysical Research: Solid Earth* **104**(B10), 23111–23125.

Skarlatoudis, A. A., P. G. Somerville, and H. K. Thio, 2016, Source-Scaling Relations of Interface Subduction Earthquakes for Strong Ground Motion and Tsunami Simulation, 106, no. 4, 1652–1662, doi: 10.1785/0120150320.

Strasser, F.O., Arango, M.C., and Bommer, J.J., 2010. Scaling of the Source Dimensions of Interface and Intraslab Subduction-zone Earthquakes with Moment Magnitude. *Seismological Research Letters* **81**(6), 941–950.

Thio, H.K., Wei, Y., Chock, G., and Li, W., 2017. Development of Offshore Probabilistic Tsunami Exceedance Amplitudes for ASCE 7-16. In Proceedings of the Sixteenth World Conference on Earthquake Engineering, Santiago.

von Huene, von, R., Miller, J.J., and Dartnell, P., 2016. A possible transoceanic tsunami directed toward the U.S. west coast from the Semidi segment, Alaska convergent margin. *Geochemistry Geophysics Geosystems* **17**(3), 645–659.

Wells, D.L., and Coppersmith, K.J., 1994. New empirical relationships among magnitude, rupture length, rupture width, rupture area, and surface displacement. *Bulletin of the Seismological Society of America* **84**(4), 974–1002.

Wesson, R.L., Boyd, O.S., Mueller, C.S., Bufe, C.G., Frankel, A.D., and Petersen, M.D., 2007. *Revision of time-independent probabilistic seismic hazard maps for Alaska*, US Geological Survey, Open File Report 2007-1043.

Witter, R.C., Briggs, R.W., and Engelhart, S.E., 2014. Little late Holocene strain accumulation and release on the Aleutian megathrust below the Shumagin Islands, Alaska. *Geophysical Research Letters*.

Ye, L., H. Kanamori, and T. Lay, 2018, Global variations of large megathrust earthquake rupture characteristics, Sci Adv, 4, no. 3, eaao4915, doi: 10.1126/sciadv.aao4915.

Appendix A Online Deliverables

The source models and codes used in in this report, as well as upcoming improvements of the probabilistic tsunami hazard codes are made available online via Github: https://github.com/hkthio/PHA

A.1 Directory structure

Currently, the site is organized as follows:

Top level:

- PHA
  - bin - executables
  - doc - manuals and reports
  - data - source models for the various subduction zones
    - Alaska
      - Sources
        - Powell-v1 - initial set of source models (superseded)
        - Powevl-v3 - improved logic tree source models (superseded)
        - Powell-v4 - the most recent set of source models, presented in this report
          - 1s_1 - single segment ruptures
          - 2s_1 - two-segment ruptures, alternative 1
          - 2s_2 - two-segment ruptures, alternative 2
          - 3s_1 - three-segment ruptures, alternative 1
          - 3s_2 - three-segment ruptures, alternative 2
          - 3s_3 - three-segment ruptures, alternative 3
          - 4s_1 - four-segment ruptures, alternative 1
          - 4s_2 - four-segment ruptures, alternative 2
          - 4s_3 - four-segment ruptures, alternative 3
          - 4s_4 - four-segment ruptures, alternative 4
          - 5s_1 - five-segment ruptures, alternative 1
          - 5s_2 - five-segment ruptures, alternative 2
          - 5s_3 - five-segment ruptures, alternative 3
  - inc - include files

- lib - compiled libraries
- src - source codes
    - PHA - probabilistic codes that are common to all types of hazard
    - PTHA - codes specific to probabilistic tsunami hazard analysis
    - PFDHA - codes specific to probabilistic fault displacement hazard
    - Misc - auxiliary libraries

A.2 File formats

A.2.1 Fault grid

The faults are approximated by a set of rectangular fault elements that are defined by centroid location (Lon/Lat/Depth), fault orientation (Strike/Dip), slip direction (Rake), Length (along strike) and Width (along dip direction). Currently, the prefix for every fault file is i_invall-, followed by the name of the source. For Alaska, the filename is i_invall-Alaska-slab2-v3, where slab2 refers to the Slab2.0 model by Hayes et al. () and v3 is a version number. Slip is in cm, there are two index numbers, one along strike (ix) and one downdip (iz).

The last index number can have different meanings depending on the application.

Longitude	Latitude	Depth	Strike	Dip	Rake	Slip	Length	Width	ix	iz	i
220.4681	60.1734	0.44	-54.8	5.3	90.0	100.00	20.70	9.06	0	0	1
220.5024	60.2615	1.28	-57.7	5.2	87.1	100.00	21.17	9.12	0	1	1
220.5366	60.3496	2.13	-60.6	5.1	84.3	100.00	21.58	9.17	0	2	1
220.5709	60.4377	2.96	-63.5	4.9	81.3	100.00	21.93	9.27	0	3	1
220.6056	60.5257	3.78	-66.8	4.7	78.0	100.00	22.24	9.38	0	4	1
220.6418	60.6139	4.58	-70.6	4.5	74.2	100.00	22.56	9.64	0	5	1
220.6782	60.7021	5.35	-74.7	4.4	70.1	100.00	22.83	9.75	0	6	1
220.6972	60.7904	6.10	-79.0	4.4	65.8	100.00	23.95	9.09	0	7	1
220.6900	60.8794	6.84	-84.4	4.3	60.4	100.00	24.76	9.00	0	8	1
220.6726	60.9687	7.59	-89.3	4.5	55.4	100.00	24.37	9.40	0	9	1
220.6551	61.0581	8.41	-93.1	4.9	51.6	100.00	24.12	9.76	0	10	1
220.6343	61.1471	9.33	-95.4	5.7	49.3	100.00	24.53	9.74	0	11	1
220.6074	61.2353	10.39	-96.7	6.6	48.0	100.00	25.83	9.67	0	12	1
220.5693	61.3225	11.60	-97.0	7.4	47.6	100.00	26.79	9.16	0	13	1
220.5225	61.4090	12.93	-97.1	8.0	47.4	100.00	26.90	9.16	0	14	1
220.4743	61.4951	14.34	-97.5	8.3	47.0	100.00	27.04	9.12	0	15	1
220.4241	61.5810	15.78	-98.7	8.4	45.8	100.00	27.09	9.19	0	16	1
220.3721	61.6666	17.23	-100.3	8.3	44.2	100.00	26.90	9.26	0	17	1
220.3182	61.7521	18.67	-100.6	8.4	43.9	100.00	27.00	9.26	0	18	1
220.2632	61.8373	20.16	-98.0	8.9	46.5	100.00	28.02	8.98	0	19	1
220.2086	61.9224	21.76	-93.1	9.9	51.4	100.00	29.72	8.70	0	20	1
220.1558	62.0075	23.52	-88.6	11.2	55.8	100.00	31.20	8.52	0	21	1
220.1051	62.0925	25.48	-85.9	12.6	58.4	100.00	31.94	8.52	0	22	1
220.0547	62.1773	27.65	-84.4	14.1	59.7	100.00	32.13	8.40	0	23	1
220.0056	62.2616	30.08	-82.6	16.1	61.2	100.00	32.01	8.47	0	24	1
220.1533	60.2734	0.48	-62.5	5.7	90.0	100.00	20.64	9.33	1	0	1
220.1770	60.3623	1.42	-65.9	5.6	86.6	100.00	21.08	9.38	1	1	1

```
220.2007   60.4512    2.35  -69.3   5.5   83.2  100.00   21.48    9.46   1    2 1
220.2247   60.5401    3.27  -72.6   5.3   79.8  100.00   21.81    9.56   1    3 1
220.2487   60.6290    4.19  -76.0   5.2   76.4  100.00   22.08    9.69   1    4 1
220.2729   60.7179    5.08  -79.4   5.1   73.0  100.00   22.27    9.85   1    5 1
220.2856   60.8066    5.96  -83.0   5.1   69.4  100.00   23.55    9.43   1    6 1
220.2708   60.8950    6.83  -86.8   5.1   65.6  100.00   24.80    8.97   1    7 1
220.2400   60.9835    7.71  -90.3   5.2   62.1  100.00   24.90    9.21   1    8 1
220.2091   61.0718    8.64  -93.0   5.6   59.4  100.00   25.09    9.41   1    9 1
220.1755   61.1598    9.68  -94.7   6.3   57.7  100.00   25.71    9.39   1   10 1
220.1353   61.2470   10.83  -95.6   7.1   56.7  100.00   26.49    9.23   1   11 1
220.0881   61.3334   12.11  -95.8   7.7   56.5  100.00   26.85    9.08   1   12 1
220.0377   61.4193   13.47  -95.6   8.2   56.6  100.00   26.98    9.07   1   13 1
219.9860   61.5050   14.90  -95.3   8.5   56.9  100.00   27.28    8.97   1   14 1
219.9318   61.5903   16.35  -94.7   8.6   57.5  100.00   27.62    8.86   1   15 1
219.8759   61.6754   17.80  -94.0   8.6   58.2  100.00   27.84    8.80   1   16 1
219.8172   61.7601   19.24  -93.0   8.5   59.2  100.00   28.32    8.59   1   17 1
219.7532   61.8439   20.66  -92.0   8.6   60.2  100.00   29.21    8.40   1   18 1
219.6859   61.9271   22.09  -91.2   8.9   60.9  100.00   30.18    8.39   1   19 1
219.6183   62.0102   23.62  -90.6   9.9   61.5  100.00   31.00    8.45   1   20 1
219.5570   62.0940   25.35  -90.2  11.1   61.9  100.00   31.22    8.82   1   21 1
219.5034   62.1787   27.31  -89.3  12.6   62.6  100.00   31.15    8.88   1   22 1
219.4538   62.2635   29.51  -88.0  14.0   63.8  100.00   31.06    8.95   1   23 1
```

A.2.2 Earthquake scenario

The earthquake scenarios are defined by filenames that are defines as follows:

Event-2-11-1-3-2-02.par – the first integer refers to the scaling relation used, the second number is the segment number, the third number is the top of the rupture branch, fourth number is the bottom of the rupture branch, fifth number is the location of the asperity and the sixth number is the sigma level for the magnitude scaling (0 = -2 sigma, 1 = -1 sigma, 2 = mean, 3 = +1 sigma and 4 is +2 sigma.

The files themselves contain the slip distribution for that particular scenario with the following information:

```
  Slip  Subfault Source          Longitude  Latitude Depth
 11.413 3013 Alaska-slab2-v3      178.4471   50.5488  7.4
 11.413 3014 Alaska-slab2-v3      178.4654   50.6353  9.8
 11.413 3015 Alaska-slab2-v3      178.4815   50.7233 11.6
 11.413 3016 Alaska-slab2-v3      178.4964   50.8120 13.0
 11.413 3017 Alaska-slab2-v3      178.5114   50.9004 14.6
 10.703 3018 Alaska-slab2-v3      178.5266   50.9878 16.7
  8.681 3019 Alaska-slab2-v3      178.5414   51.0738 19.5
  6.268 3020 Alaska-slab2-v3      178.5549   51.1583 22.9
 11.413 3024 Alaska-slab2-v3      178.1681   50.5848  7.4
 11.413 3025 Alaska-slab2-v3      178.1902   50.6710  9.8
 11.413 3026 Alaska-slab2-v3      178.2094   50.7588 11.6
 11.413 3027 Alaska-slab2-v3      178.2269   50.8472 13.0
 11.413 3028 Alaska-slab2-v3      178.2445   50.9354 14.6
 10.743 3029 Alaska-slab2-v3      178.2624   51.0224 16.9
  8.694 3030 Alaska-slab2-v3      178.2798   51.1081 19.7
  6.278 3031 Alaska-slab2-v3      178.2957   51.1922 23.1
 11.413 3035 Alaska-slab2-v3      177.8902   50.6244  7.3
 11.413 3036 Alaska-slab2-v3      177.9160   50.7103  9.7
 11.413 3037 Alaska-slab2-v3      177.9384   50.7977 11.5
 11.413 3038 Alaska-slab2-v3      177.9585   50.8859 12.9
```

```
 11.413 3039 Alaska-slab2-v3      177.9788   50.9738 14.6
 10.775 3040 Alaska-slab2-v3      177.9995   51.0605 16.9
  8.700 3041 Alaska-slab2-v3      178.0197   51.1457 19.8
  6.254 3042 Alaska-slab2-v3      178.0379   51.2295 23.2
 11.413 3046 Alaska-slab2-v3      177.6130   50.6669  7.3
 11.413 3047 Alaska-slab2-v3      177.6429   50.7524  9.6
 11.413 3048 Alaska-slab2-v3      177.6686   50.8395 11.3
 11.413 3049 Alaska-slab2-v3      177.6915   50.9274 12.8
 11.413 3050 Alaska-slab2-v3      177.7145   51.0150 14.5
 10.807 3051 Alaska-slab2-v3      177.7381   51.1013 16.8
  8.708 3052 Alaska-slab2-v3      177.7610   51.1862 19.8
  6.238 3053 Alaska-slab2-v3      177.7817   51.2696 23.2
  9.273 3057 Alaska-slab2-v3      177.3364   50.7120  7.2
  9.273 3058 Alaska-slab2-v3      177.3704   50.7972  9.4
  9.273 3059 Alaska-slab2-v3      177.3997   50.8839 11.2
  9.273 3060 Alaska-slab2-v3      177.4254   50.9714 12.7
  9.273 3061 Alaska-slab2-v3      177.4512   51.0587 14.4
  8.803 3062 Alaska-slab2-v3      177.4776   51.1447 16.7
```

A.2.3 Rate tables

The rate table (Events.table) has the following format:

```
Scenario name       Rate (1/yr)  Magnitude      → not used
Event-1-01-1-1-1-02 0.543006E-05 9.124          9999.0 1 1   0.0   0.0
Event-1-01-1-1-2-02 0.543006E-05 9.124          9999.0 2 1   0.0   0.0
Event-1-01-1-1-3-02 0.543006E-05 9.124          9999.0 3 1   0.0   0.0
Event-1-01-1-2-1-02 0.108601E-04 9.124          9999.0 1 1   0.0   0.0
Event-1-01-1-2-2-02 0.108601E-04 9.124          9999.0 2 1   0.0   0.0
Event-1-01-1-2-3-02 0.108601E-04 9.124          9999.0 3 1   0.0   0.0
Event-1-01-1-3-1-02 0.543006E-05 9.124          9999.0 1 1   0.0   0.0
Event-1-01-1-3-2-02 0.543006E-05 9.124          9999.0 2 1   0.0   0.0
Event-1-01-1-3-3-02 0.543006E-05 9.124          9999.0 3 1   0.0   0.0
Event-1-01-2-1-1-02 0.749908E-05 8.917          9999.0 1 1   0.0   0.0
Event-1-01-2-1-2-02 0.749908E-05 8.917          9999.0 2 1   0.0   0.0
Event-1-01-2-1-3-02 0.749908E-05 8.917          9999.0 3 1   0.0   0.0
Event-1-01-2-2-1-02 0.149982E-04 8.917          9999.0 1 1   0.0   0.0
Event-1-01-2-2-2-02 0.149982E-04 8.917          9999.0 2 1   0.0   0.0
Event-1-01-2-2-3-02 0.149982E-04 8.917          9999.0 3 1   0.0   0.0
Event-1-01-2-3-1-02 0.749908E-05 8.917          9999.0 1 1   0.0   0.0
Event-1-01-2-3-2-02 0.749908E-05 8.917          9999.0 2 1   0.0   0.0
Event-1-01-2-3-3-02 0.749908E-05 8.917          9999.0 3 1   0.0   0.0
Event-1-02-1-1-1-02 0.942494E-05 9.236          9999.0 1 2   0.0   0.0
Event-1-02-1-1-2-02 0.942494E-05 9.236          9999.0 2 2   0.0   0.0
Event-1-02-1-1-3-02 0.942494E-05 9.236          9999.0 3 2   0.0   0.0
Event-1-02-1-2-1-02 0.138041E-04 9.435          9999.0 1 2   0.0   0.0
Event-1-02-1-2-2-02 0.138041E-04 9.435          9999.0 2 2   0.0   0.0
Event-1-02-1-2-3-02 0.138041E-04 9.435          9999.0 3 2   0.0   0.0
Event-1-02-1-3-1-02 0.517369E-05 9.619          9999.0 1 2   0.0   0.0

Scenario name       Mag   Original rate New rate
Event-1-01-1-1-1-02 9.124 5.430060e-06 6.005709e-06
Event-1-01-1-1-2-02 9.124 5.430060e-06 5.557542e-06
Event-1-01-1-1-3-02 9.124 5.430060e-06 5.167238e-06
```

```
Event-1-01-1-2-1-02 9.124 1.086010e-05 1.107443e-05
Event-1-01-1-2-2-02 9.124 1.086010e-05 1.151207e-05
Event-1-01-1-2-3-02 9.124 1.086010e-05 1.163911e-05
Event-1-01-1-3-1-02 9.124 5.430060e-06 5.343682e-06
Event-1-01-1-3-2-02 9.124 5.430060e-06 5.202262e-06
Event-1-01-1-3-3-02 9.124 5.430060e-06 5.808644e-06
Event-1-01-2-1-1-02 8.917 7.499080e-06 6.750834e-06
Event-1-01-2-1-2-02 8.917 7.499080e-06 8.033547e-06
Event-1-01-2-1-3-02 8.917 7.499080e-06 8.127427e-06
Event-1-01-2-2-1-02 8.917 1.499820e-05 1.597762e-05
Event-1-01-2-2-2-02 8.917 1.499820e-05 1.498349e-05
Event-1-01-2-2-3-02 8.917 1.499820e-05 1.472185e-05
Event-1-01-2-3-1-02 8.917 7.499080e-06 8.334848e-06
Event-1-01-2-3-2-02 8.917 7.499080e-06 8.102384e-06
Event-1-01-2-3-3-02 8.917 7.499080e-06 7.891410e-06
Event-1-02-1-1-1-02 9.236 9.424940e-06 8.618702e-06
Event-1-02-1-1-2-02 9.236 9.424940e-06 8.528987e-06
Event-1-02-1-1-3-02 9.236 9.424940e-06 1.039025e-05
Event-1-02-1-2-1-02 9.435 1.380410e-05 1.507437e-05
Event-1-02-1-2-2-02 9.435 1.380410e-05 1.362898e-05
```

A.3 Software

The software used to develop the source representation and the scenarios are also available on the Github site. The PTHA software is part of a larger framework that included fault displacement hazard codes as well as (in the future) seismic hazard codes, which are also accessible. These codes are in development, the older working codes used for this report are outlined below.

A.3.1 Gridding of the source

In order to develop a more accurate representation of the sources, we can generate the grid in two stages; an initial gridding with very high resolution (e.g., 2kmx1km) that is then resampled to a more manageable size (e.g., 50kmx25km). The coarser grid can be used to compute the probabilistic model while using the high-resolution grid to compute the displacement Green's function to account for complexities in the source geometry (e.g., curvature along strike as well as down-dip).

- cont2grid.c - code to develop source grids from depth contour lines of the fault
- Resample_Invall-v1.1.c - resampling to a coarser grid

A.3.2 Generating probabilistic sources

Currently, a single Fortran code is used to compute the probabilistic scenarios:

- GetRupMod-v2.4.f - code to develop slip distributions and rates of occurrence for a logic tree model

Code input:

```
v2.3
Alaska-slab2-v3
Alaska-slab2-v3
-2              : nTop
```

```
.50 .50          : wtTop
-3               : nBot
.20 .60 .20      : wtBot
8                : nLen
0   11  30  64  88  110 144 180 : iStart
10  29  63  87  109 143 179 205 : iEnd
.21 .12 .12 .12 .12 .12 .12 .12 : wtLen
57  59  63  69  71  70  59  47  : Rate
.5  1.  1.  .02 .7  1.  .5  1.  : Coupling
0   0   0   0   0   14  0   0   : zTop 1
8   8   8   8   14  28  8   8   : zTop 2
32  15  20  15  16  25  25  10  : zBot 1
37  22  30  20  22  35  30  12  : zBot 2
42  35  40  30  30  42  35  17  : zBot 3
32e9             : Mu
3 2.0            : Asperity step, DmaxDav
```

Appendix B Complete logic trees

B.1 Overall logic tree

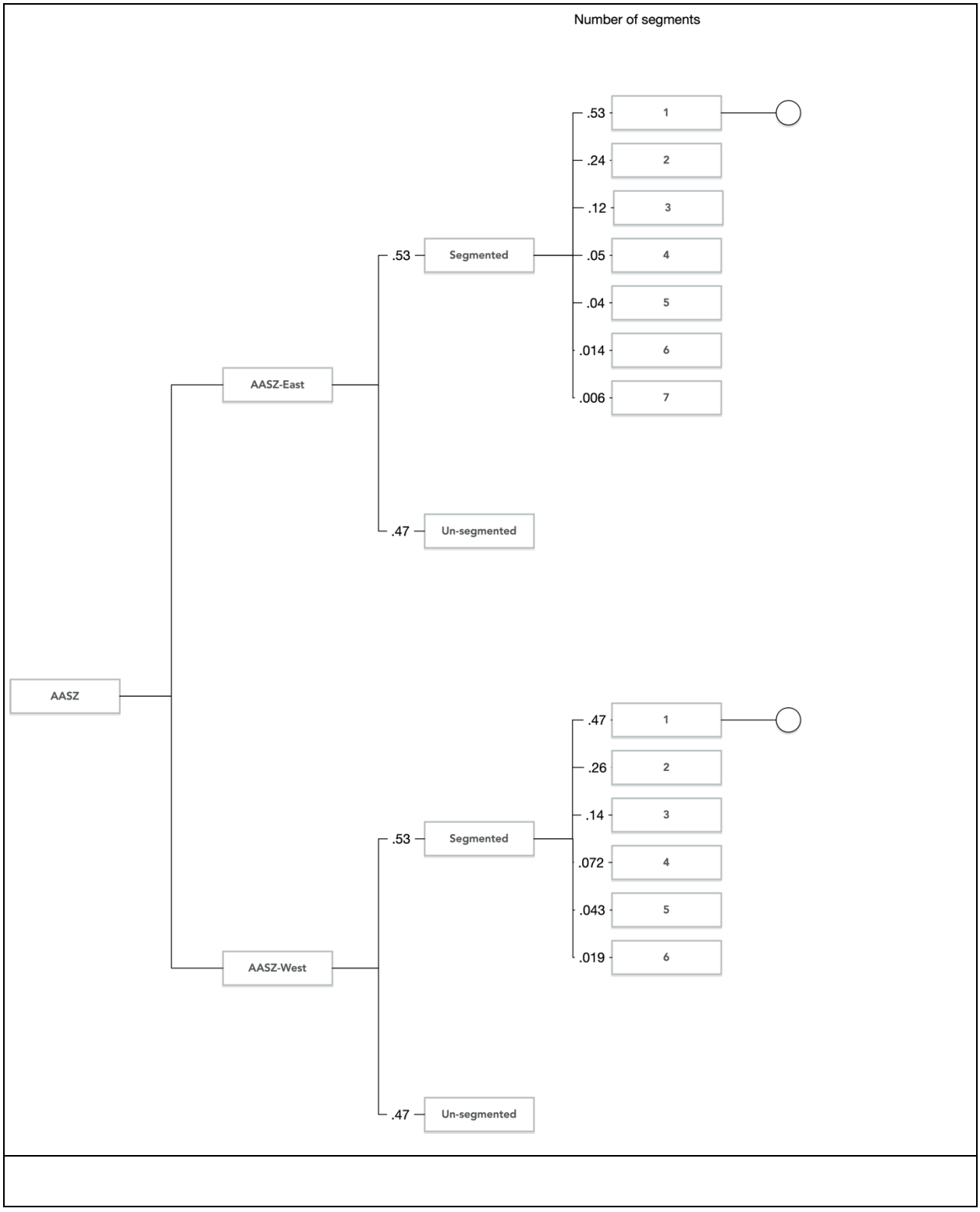

B.2 Eastern AASZ

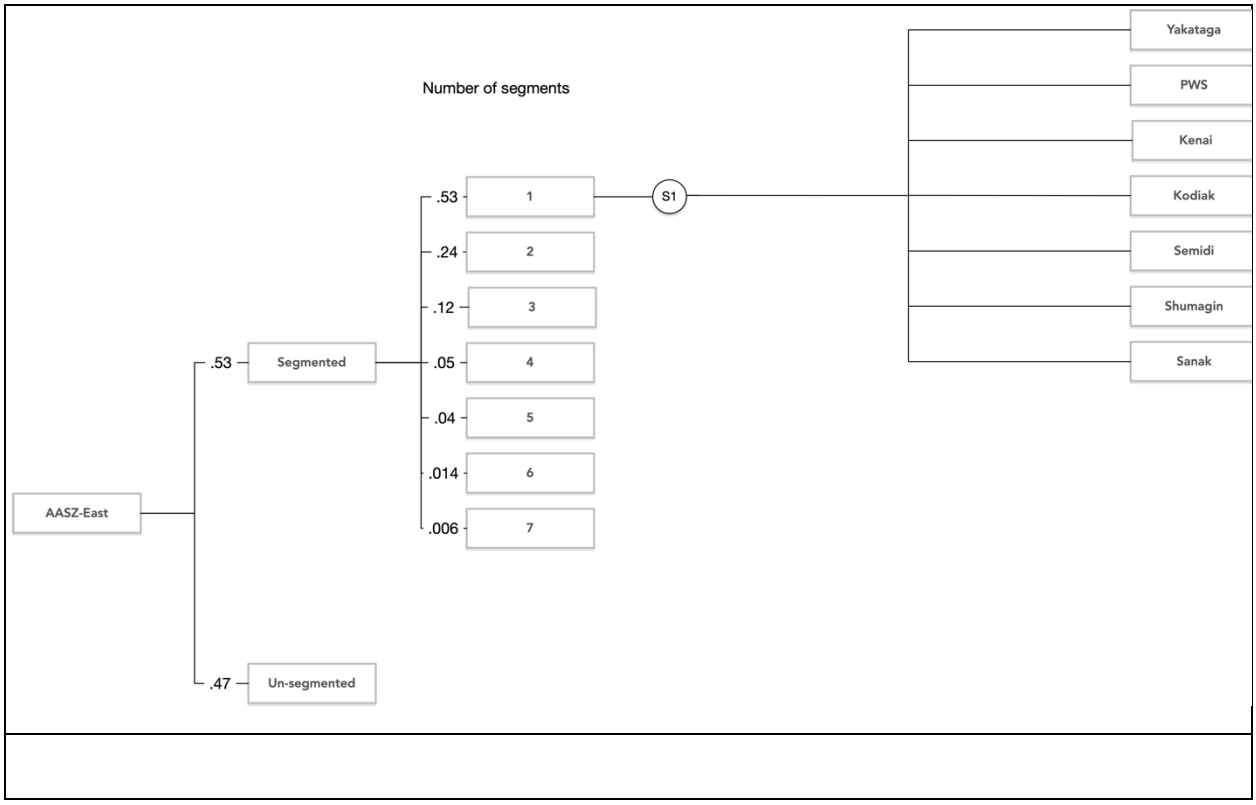

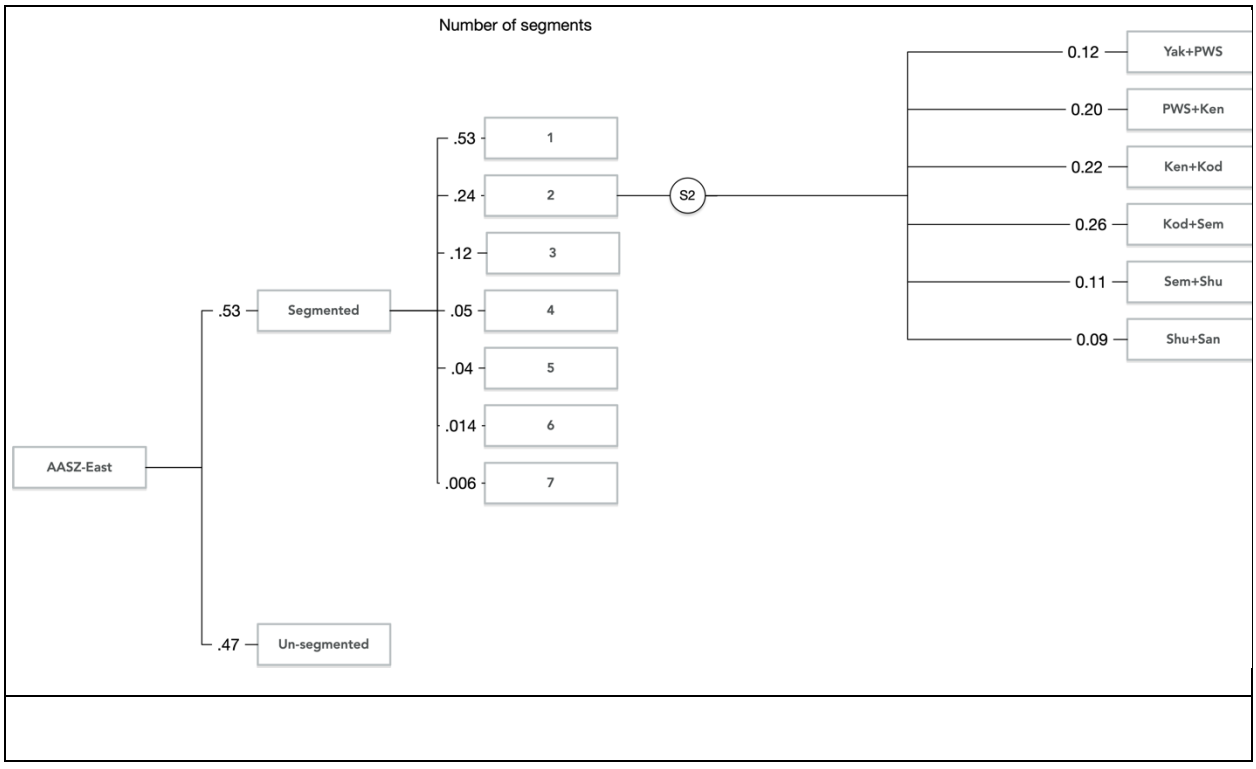

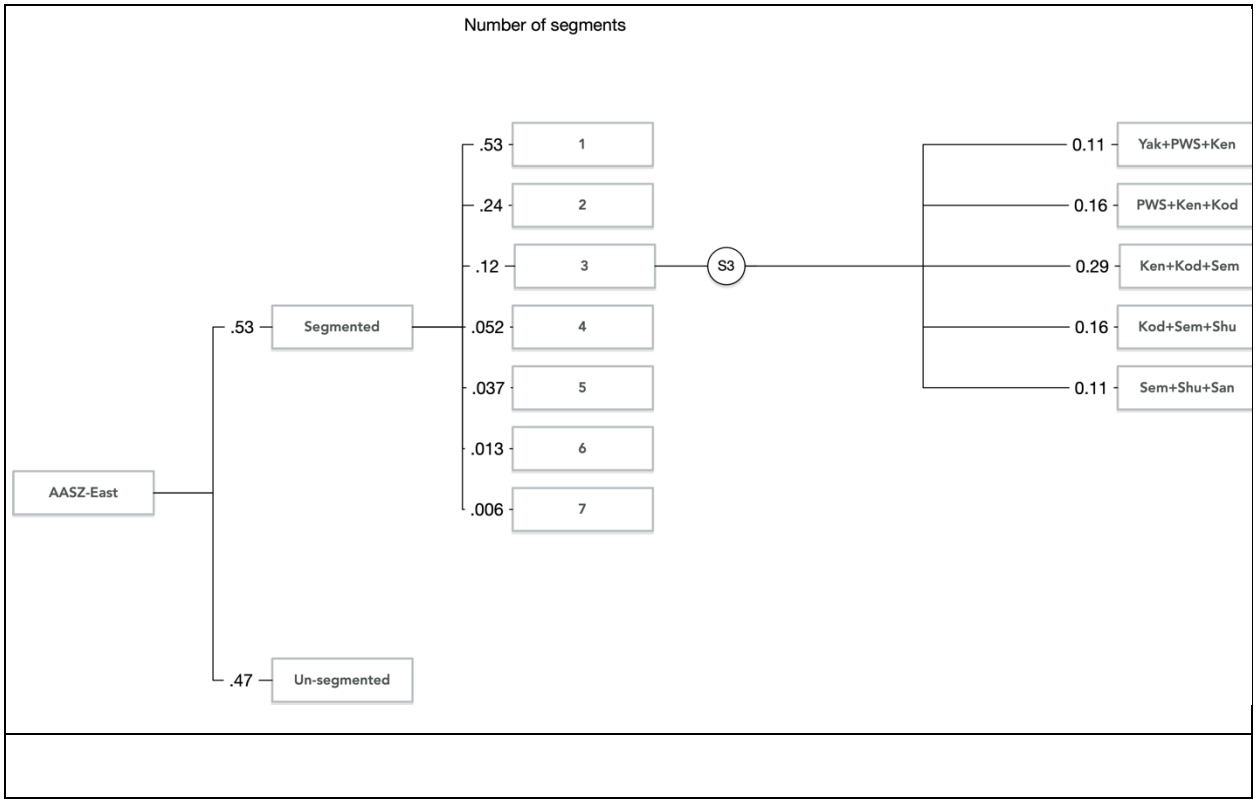
Number of segments
AASZ-East
.53
Segmented
.47
Un-segmented
.53
1
.24
2
.12
3
.052
4
.037
5
.013
6
.006
7
S3
0.11
Yak+PWS+Ken
0.16
PWS+Ken+Kod
0.29
Ken+Kod+Sem
0.16
Kod+Sem+Shu
0.11
Sem+Shu+San

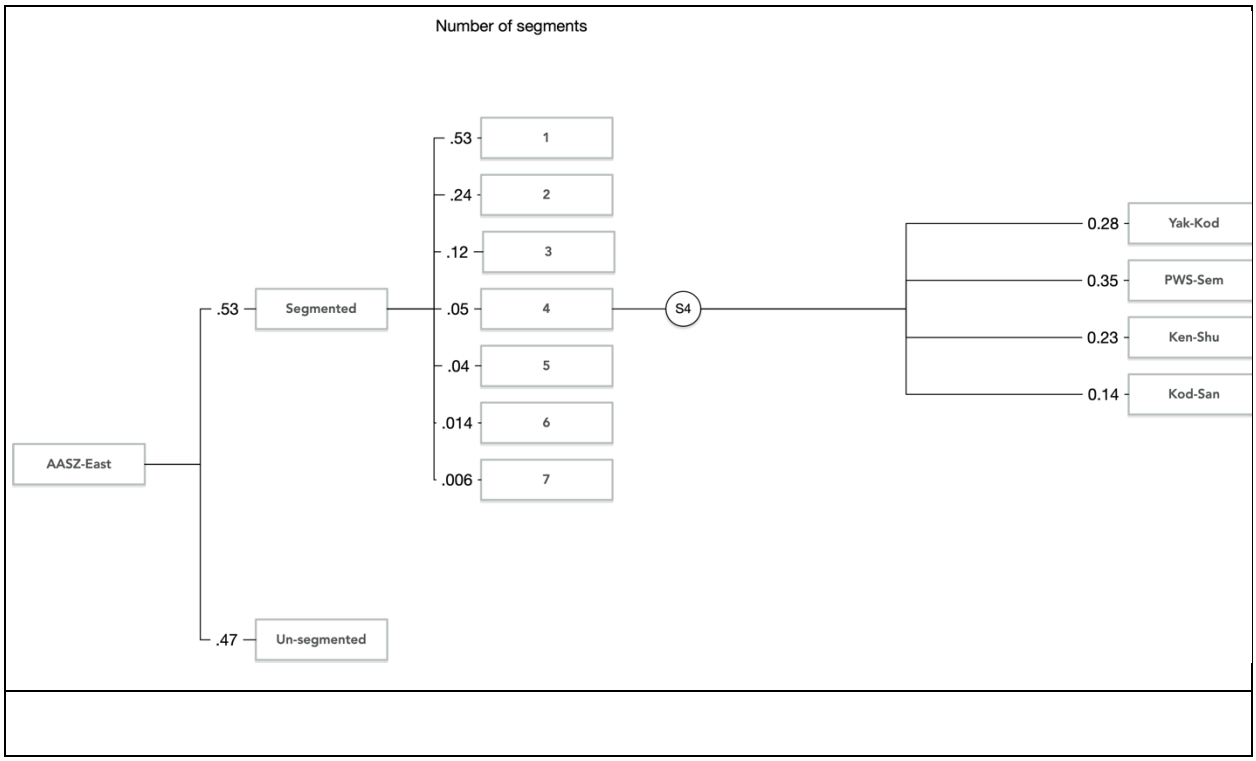
Number of segments
AASZ-East
.53
Segmented
.47
Un-segmented
.53
1
.24
2
.12
3
.05
4
.04
5
.014
6
.006
7
S4
0.28
Yak-Kod
0.35
PWS-Sem
0.23
Ken-Shu
0.14
Kod-San

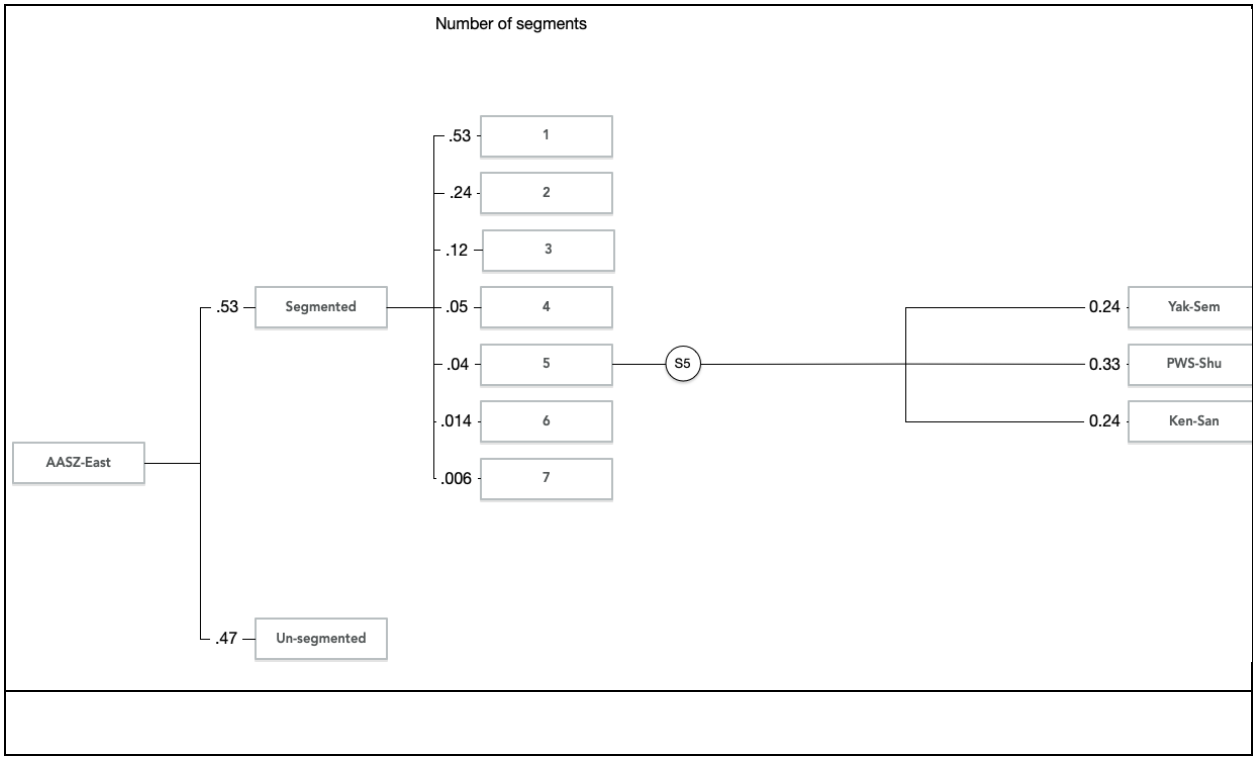
Number of segments
AASZ-East
.53
Segmented
.47
Un-segmented
.53
1
.24
2
.12
3
.05
4
.04
5
.014
6
.006
7
S5
0.24
Yak-Sem
0.33
PWS-Shu
0.24
Ken-San

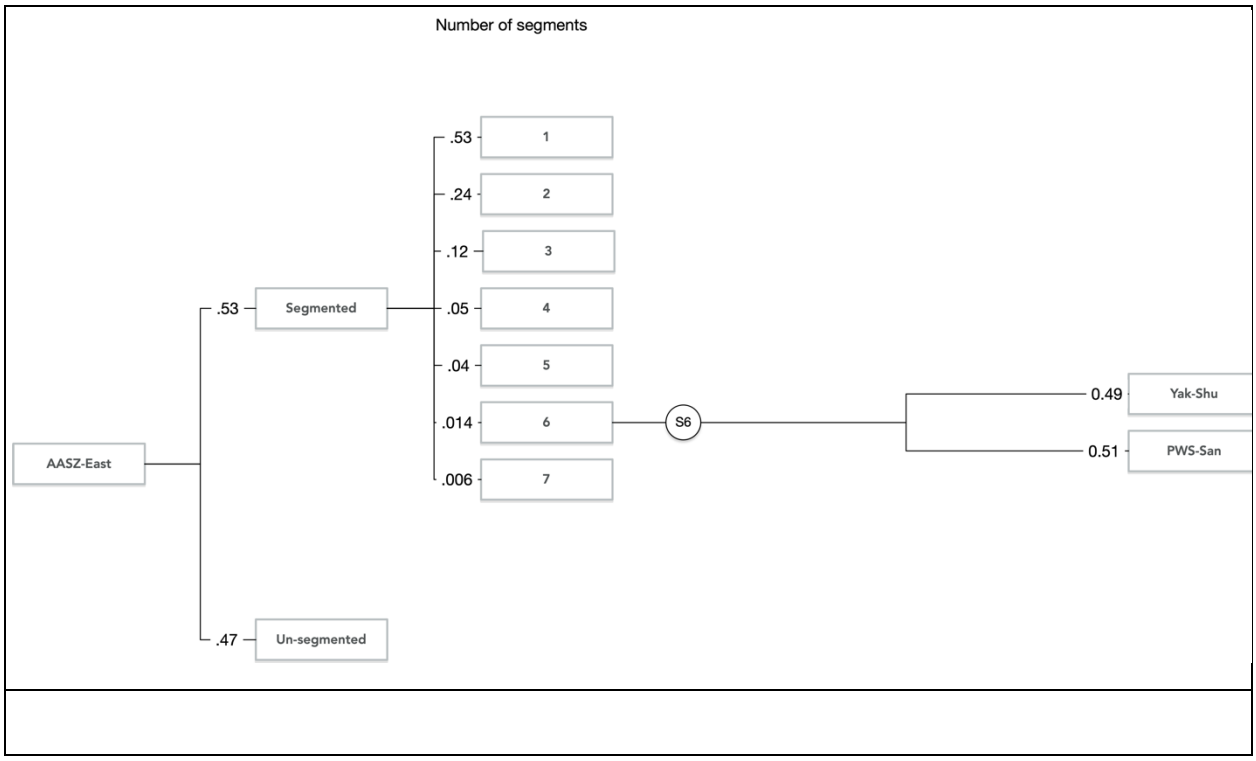
Number of segments
AASZ-East
.53
Segmented
.47
Un-segmented
.53
1
.24
2
.12
3
.05
4
.04
5
.014
6
.006
7
S6
0.49
Yak-Shu
0.51
PWS-San

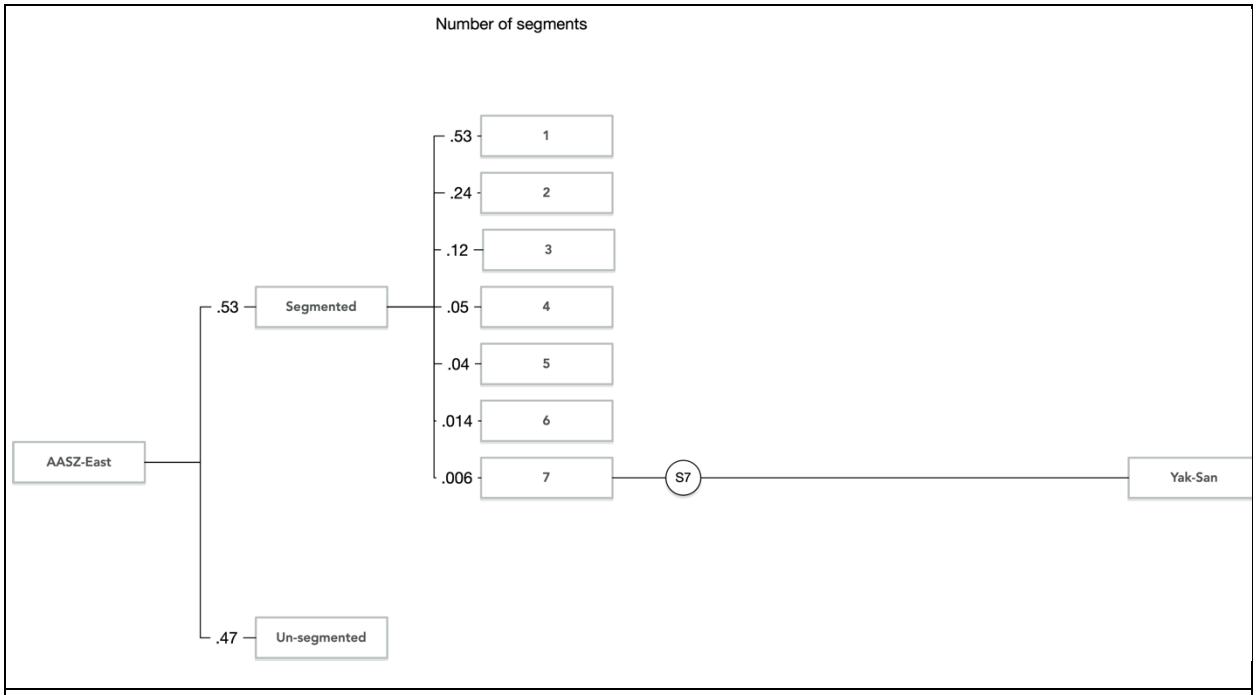
Number of segments
AASZ-East
.53
Segmented
.47
Un-segmented
.53
1
.24
2
.12
3
.05
4
.04
5
.014
6
.006
7
S7
Yak-San

B.3 Western AASZ

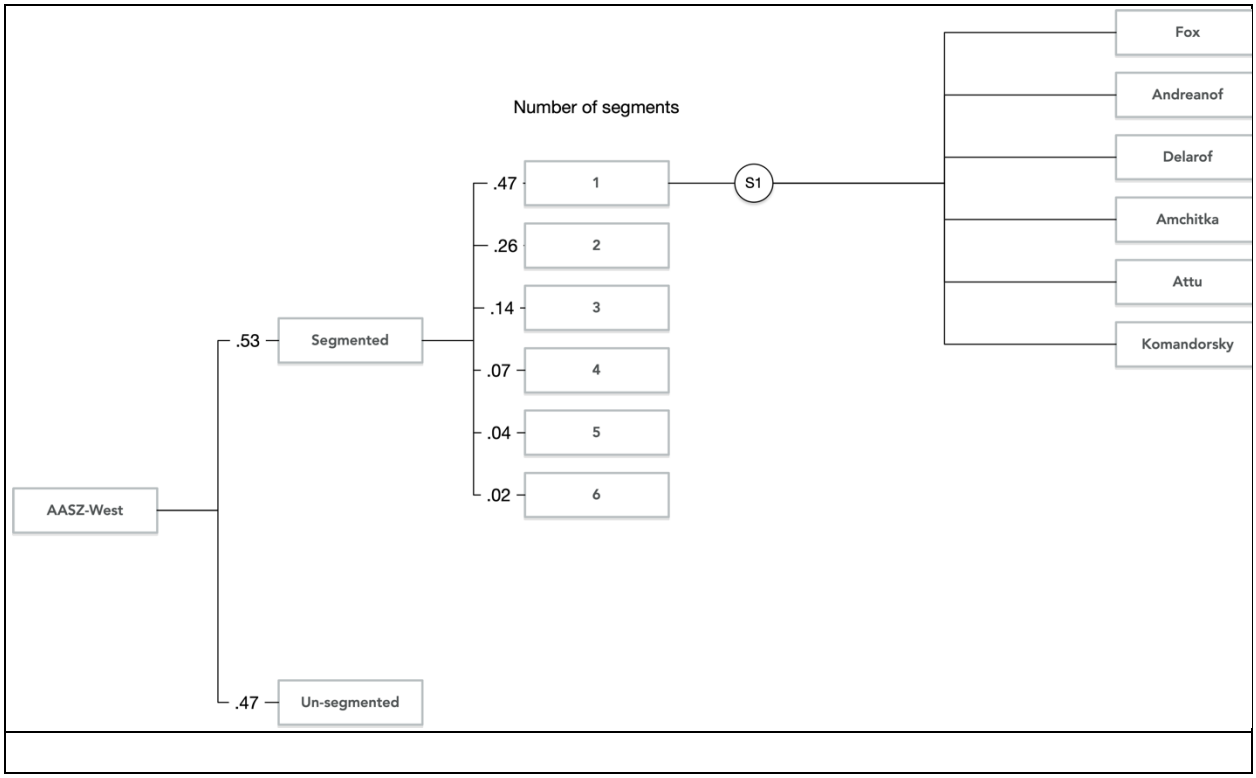

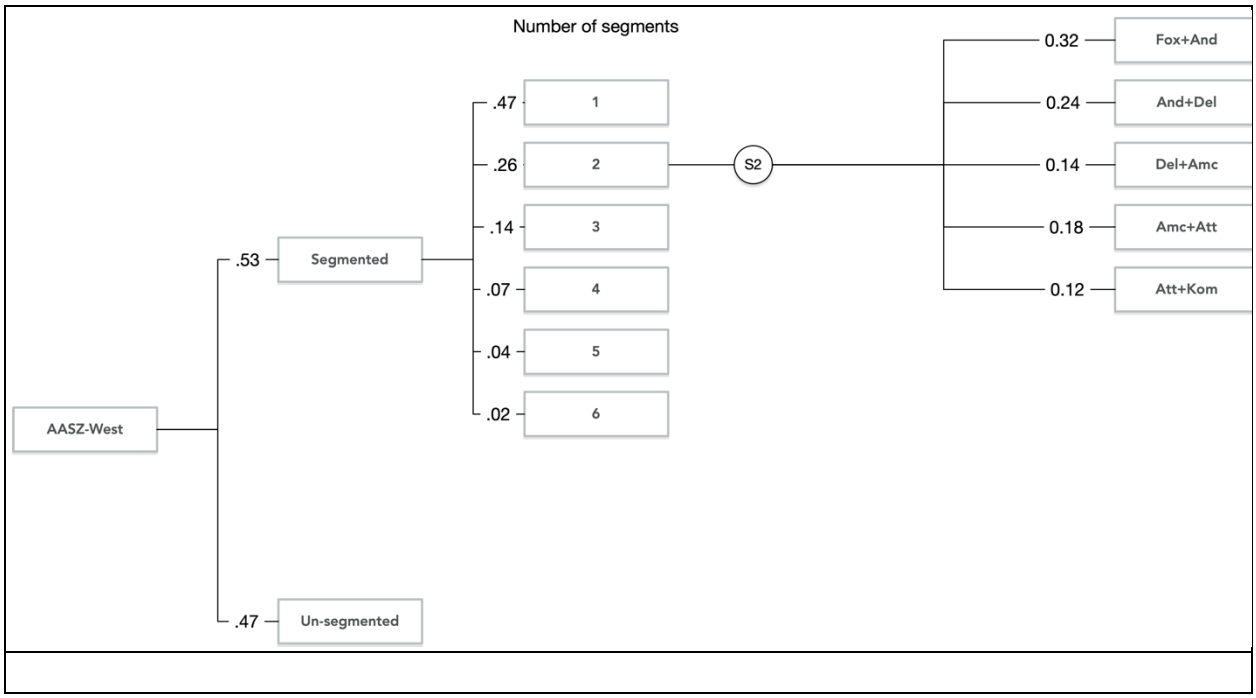

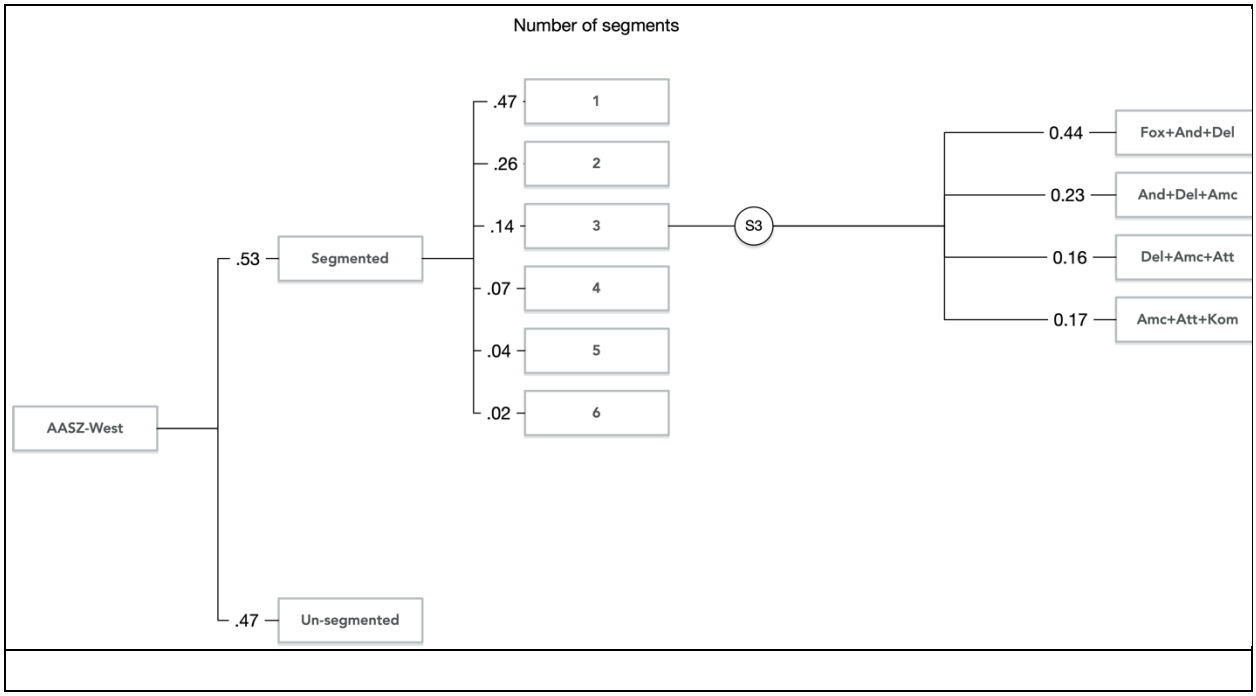
Number of segments
AASZ-West
.53
Segmented
.47
Un-segmented
.47
1
.26
2
.14
3
.07
4
.04
5
.02
6
S3
0.44
Fox+And+Del
0.23
And+Del+Amc
0.16
Del+Amc+Att
0.17
Amc+Att+Kom

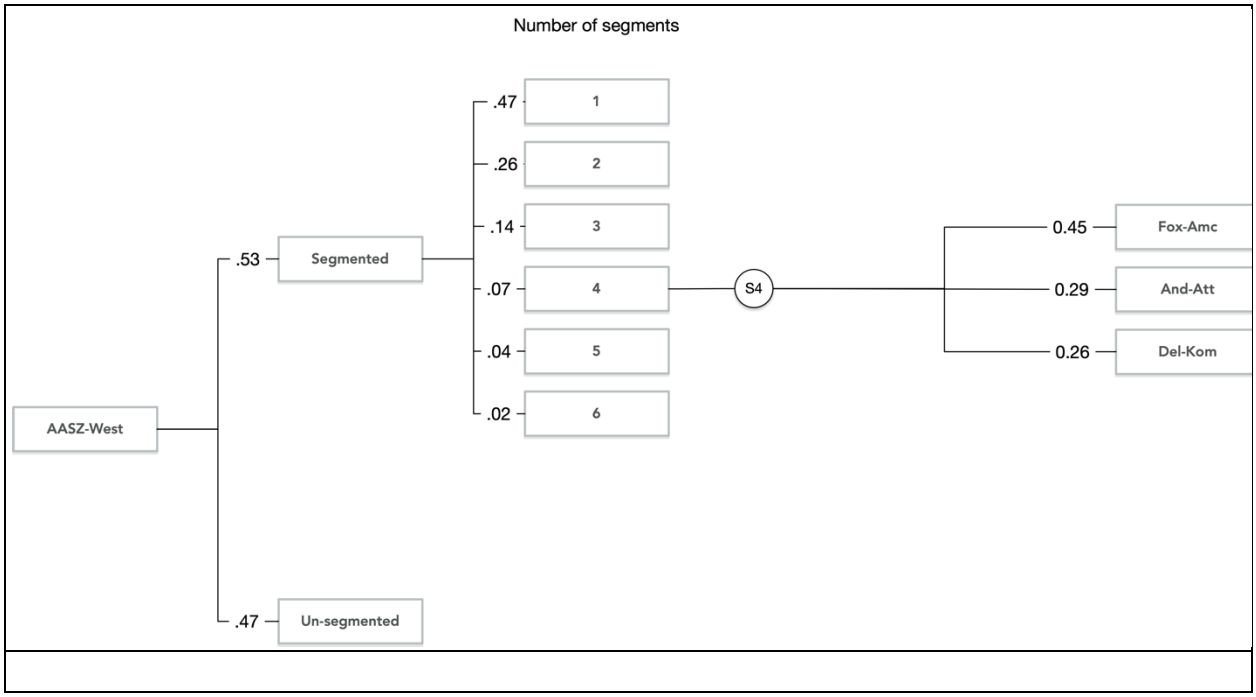
Number of segments
AASZ-West
.53
Segmented
.47
Un-segmented
.47
1
.26
2
.14
3
.07
4
.04
5
.02
6
S4
0.45
Fox-Amc
0.29
And-Att
0.26
Del-Kom

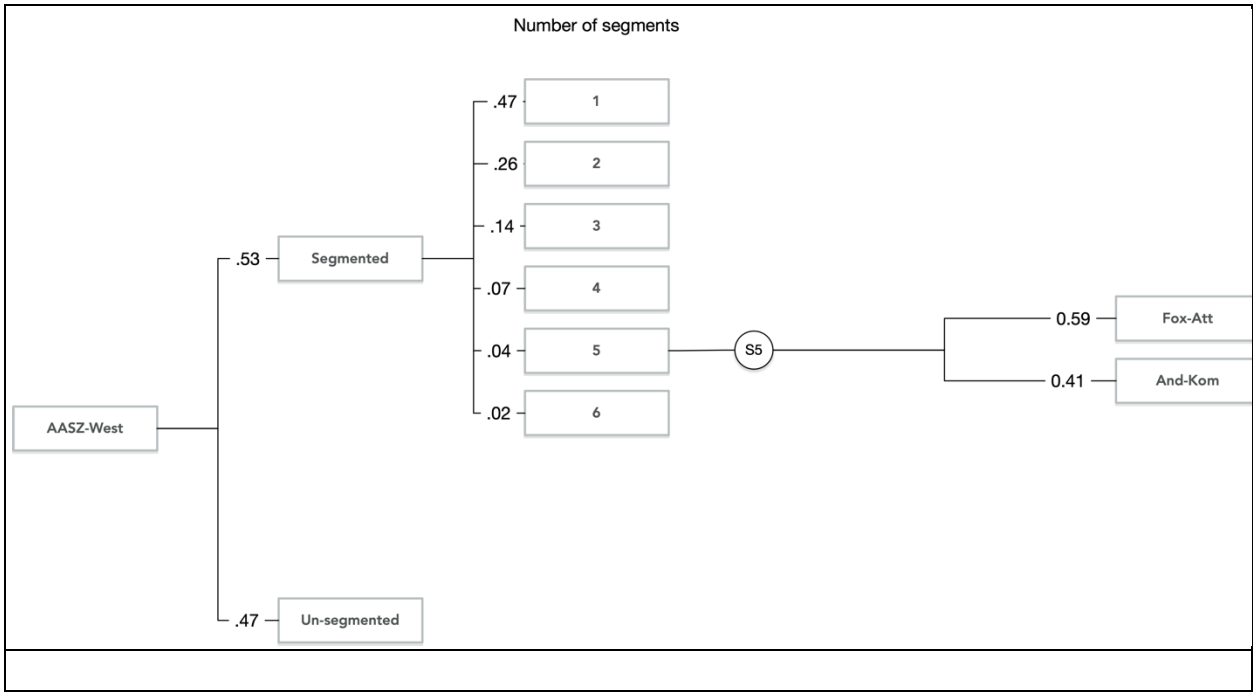
Number of segments
.47
1
.26
2
.14
3
.53
Segmented
.07
4
.04
5
S5
0.59
Fox-Att
0.41
And-Kom
AASZ-West
.02
6
.47
Un-segmented

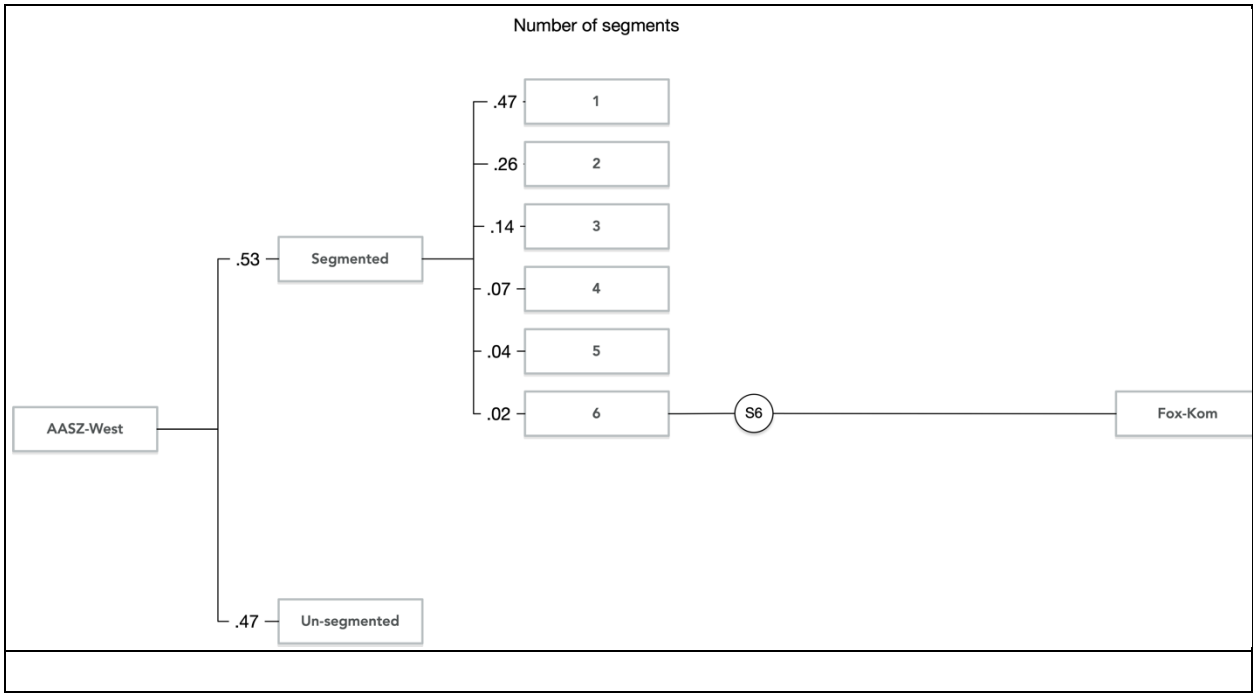
Number of segments
.47
1
.26
2
.14
3
.53
Segmented
.07
4
.04
5
AASZ-West
.02
6
S6
Fox-Kom
.47
Un-segmented